
Universiteit
Leiden
The Netherlands

A family of bacterial Josephin-like deubiquitinases with an irreversible cleavage mode

Hermanns, T.; Kolek, S.; Uthoff, M.; Heiden, R.A. de; Mulder, M.P.C.; Baumann, U.; Hofmann, K.

Citation
Hermanns, T., Kolek, S., Uthoff, M., Heiden, R. A. de, Mulder, M. P. C., Baumann, U., & Hofmann, K. (2025). A family of bacterial Josephin-like deubiquitinases with an irreversible cleavage mode. *Molecular Cell*, *85*(6), 1202-1215. doi:10.1016/j.molcel.2025.02.002

Version:	Publisher's Version
License:	Creative Commons CC BY 4.0 license
Downloaded from:	https://hdl.handle.net/1887/4293415

Note: To cite this publication please use the final published version (if applicable).

Molecular Cell

Article

A family of bacterial Josephin-like deubiquitinases with an irreversible cleavage mode

Graphical abstract

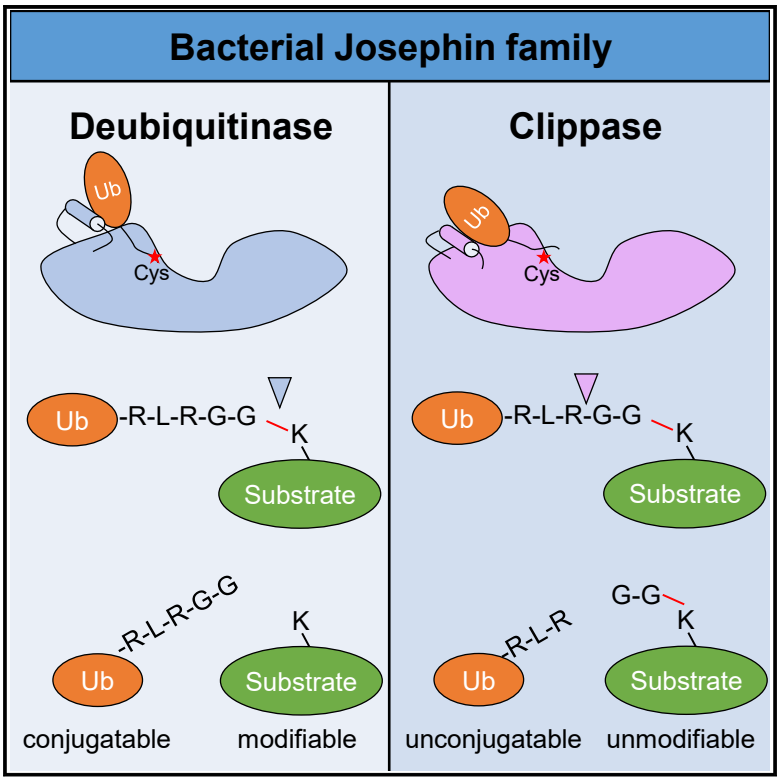

Highlights

- Bacteria from diverse taxa encode deubiquitinase effectors of the Josephin family
- Many bacterial Josephins have clippase activity and cleave ubiquitin after Arg-74
- Clippase activity makes deubiquitination irreversible by destroying ubiquitin
- Clippases and conventional Josephin DUBs bind ubiquitin in different orientations

Authors

Thomas Hermanns, Susanne Kolek, Matthias Uthoff, Richard A. de Heiden, Monique P.C. Mulder, Ulrich Baumann, Kay Hofmann

Correspondence

kay.hofmann@uni-koeln.de

In brief

Many intracellular bacteria secrete deubiquitinase effectors into the host cell, inhibiting ubiquitin-based host defenses. Hermanns et al. show that one family of bacterial effectors can cleave ubiquitin after Arg-74, thereby making the deubiquitination irreversible. The shifted cleavage site is caused by a different ubiquitin-recognition mode.

Hermanns et al., 2025, Molecular Cell *85*, 1202–1215
March 20, 2025 © 2025 The Author(s). Published by Elsevier Inc.
https://doi.org/10.1016/j.molcel.2025.02.002

CellPress

CellPress
OPEN ACCESS

Molecular Cell

Article

A family of bacterial Josephin-like deubiquitinases with an irreversible cleavage mode

Thomas Hermanns,[1] Susanne Kolek,[1] Matthias Uthoff,[2,4] Richard A. de Heiden,[3] Monique P.C. Mulder,[3] Ulrich Baumann,[2] and Kay Hofmann[1,5,*]

[1]Institute for Genetics, University of Cologne, Zülpicher Straße 47a, 50674 Cologne, Germany
[2]Institute of Biochemistry, University of Cologne, Zülpicher Straße 47, 50674 Cologne, Germany
[3]Department of Cell and Chemical Biology, Leiden University Medical Center (LUMC), Einthovenweg 20, 2333ZC Leiden, the Netherlands
[4]Present address: Bayer AG, Research & Development, Pharmaceuticals, Biologics Research, Aprather Weg 18a, 42113 Wuppertal, Germany
[5]Lead contact
*Correspondence: kay.hofmann@uni-koeln.de
https://doi.org/10.1016/j.molcel.2025.02.002

SUMMARY

Many intracellular bacteria secrete deubiquitinase (DUB) effectors into eukaryotic host cells to keep the bacterial surface or the enclosing vesicle membrane free of ubiquitin marks. This study describes a family of DUBs from several bacterial genera, including *Simkania*, *Parachlamydia*, *Burkholderia*, and *Pigmentiphaga*, which is structurally related to eukaryotic Josephin-type DUBs but contains members that catalyze a unique destructive substrate deubiquitination. These ubiquitin C-terminal clippases (UCCs) cleave ubiquitin before the C-terminal diGly motif, thereby truncating the modifier and leaving a remnant on the substrate. By comparing the crystal structures of substrate-bound clippases and a closely related conventional DUB, we identified the factors causing this shift and found them to be conserved in other clippases, including one highly specific for M1-linked ubiquitin chains. This enzyme class has great potential to serve as tools for studying the ubiquitin system, particularly aspects involving branched chains.

INTRODUCTION

Protein ubiquitination is a post-translational modification that regulates many aspects of eukaryotic cell biology, including the defense against intracellular pathogens. Through a cascade of ubiquitin-activating, conjugating, and ligating enzymes, the C terminus of ubiquitin is covalently attached to a substrate, usually via an isopeptide linkage to the ε-amino group of a substrate lysine, but occasionally to the N terminus or to serine or threonine side chains.[1] Since substrate-attached ubiquitin can be ubiquitinated on several lysines, chains of different linkage types are generated, which confer different fates on the modified substrates. Ubiquitination can be reversed through the action of deubiquitinases (DUBs), which specifically cleave isopeptide or peptide bonds formed by the C terminus of ubiquitin, thereby restoring both ubiquitin and the substrate to their original, unmodified state, with the possibility of later re-ubiquitination through the ubiquitin-conjugating cascade.[2]

Although bacteria lack a ubiquitin system of their own, many pathogenic or symbiotic bacteria have evolved ubiquitin-directed effectors that are secreted into the host cell and increase bacterial fitness by interfering with host defense pathways.[3–5] Bacterial ubiquitin ligases can modify host proteins with K48- or K11-linked ubiquitin chains, thereby targeting them for proteasomal degradation.[6] On the other hand, host cells use their own ligases to install ubiquitin on the surface of invading bacteria or on the surface of bacteria-containing vacuoles (BCVs), in which some intracellular bacteria are shielded from direct cytoplasmic access.[7] In the absence of bacterial countermeasures, this surface-bound ubiquitin targets bacterial particles for xenophagy or directs ubiquitinated BCVs toward lysosomal degradation.[8] Bacteria with intracellular lifestyles have evolved mechanisms to evade this fate, either by preventing ligase access to the bacteria,[9] by interfering with ubiquitination,[10] or—most prominently—by using DUB effectors to remove previously attached ubiquitin.[3,11,12] Most bacterial DUBs appear to be recent acquisitions from host genomes, since they show recognizable sequence and structural similarity to eukaryotic DUBs and are often restricted to narrow bacterial taxa. More distantly related bacteria often encode DUBs that result from independent acquisition events. Apart from a small metalloprotease family, all eukaryotic DUBs are papain-fold cysteine proteases, which can be grouped into seven different classes (USP, UCH, OTU, Josephin, MINDY, ZUFSP, and VTD).[2,13] Most bacterial DUBs are either related to the OTU (ovarian tumor) family[14] or belong to the so-called CE-clan, an enzyme family comprising eukaryotic proteases for the ubiquitin-like modifiers SUMO and NEDD8 and bacterial deubiquitinating enzymes.[15] Typical

 © 2025 The Author(s). Published by Elsevier Inc.
This is an open access article under the CC BY license (http://creativecommons.org/licenses/by/4.0/).

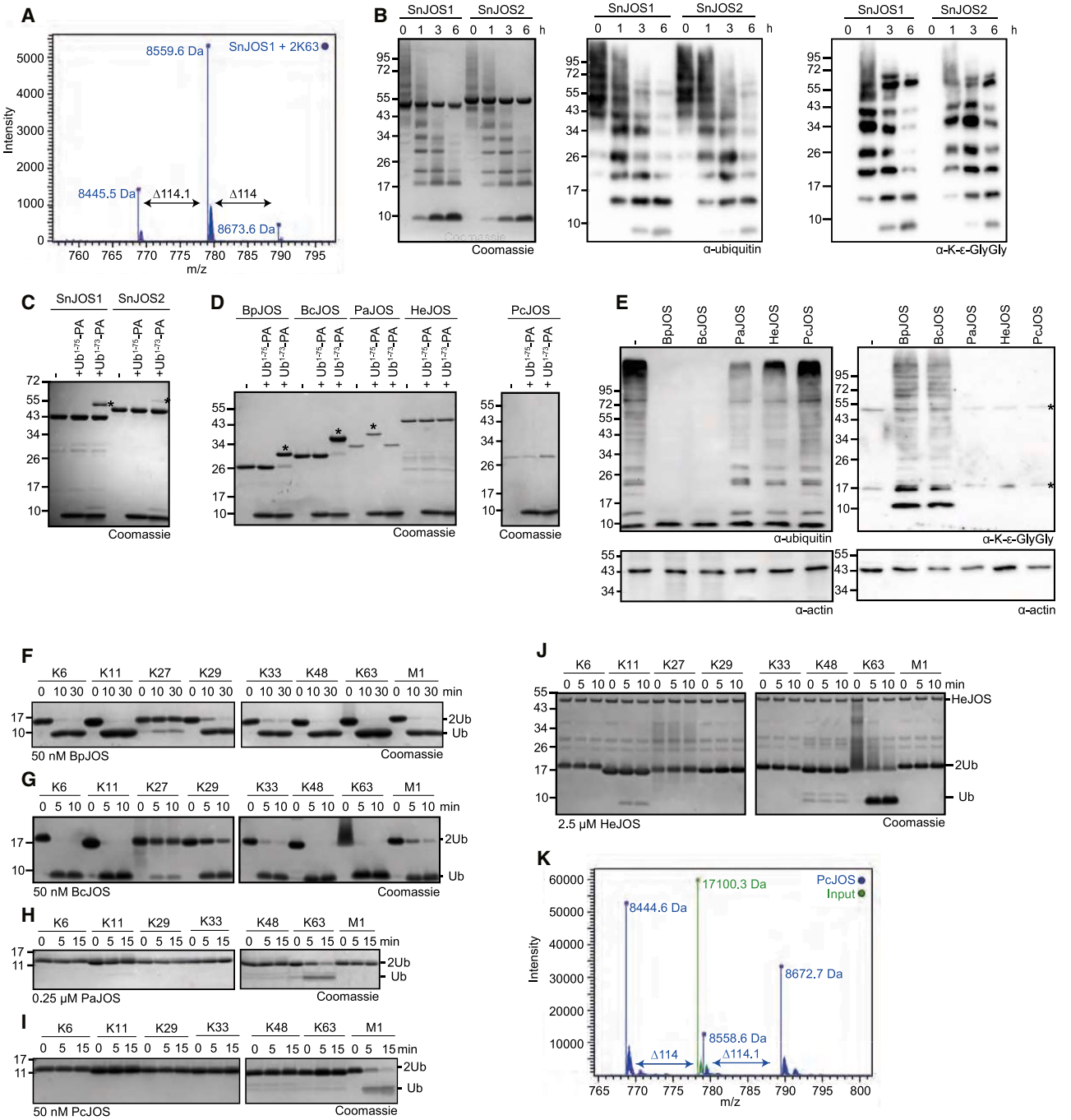

Figure 1. Bacterial Josephins cleave ubiquitin at different positions

(A) Intact mass spectrometry of K63-linked diubiquitin cleaved by SnJOS1. The x axis shows *m/z* ratio, with deconvoluted masses next to peaks. The 8,559.6 Da peak corresponds to mono-ubiquitin, while other peaks differ by 114 Da, indicating GlyGly-peptide removal/addition.

(B) Analysis of SnJOS1/2 cleavage products by western blotting. K63-linked Ub6+ chains were incubated with 5 μM SnJOS1 or SnJOS2 for indicated times. Poly-ubiquitin chain degradation is visualized by Coomassie-staining and α-ubiquitin western blotting. GlyGly-remnant accumulation is shown by α-K-ε-GlyGly detection.

(C) Cleavage position determination using activity-based probes. SnJOS1 and SnJOS2 were incubated with $Ub^{1–75}$ or $Ub^{1–73}$-PA probes for 18 h. Asterisks (*) mark shifted bands after reaction.

(D) Differential probe reactivity of additional bacterial Josephin homologs, performed as in (C).

(legend continued on next page)

intracellular bacteria such as *Salmonella typhimurium*, *Shigella flexneri*, *Burkholderia pseudomallei*, *Chlamydia pneumoniae*, and *Chlamydia trachomatis* encode one or two DUBs, usually members of the OTU or CE family, with little linkage specificity.[11] Two exceptions are *Legionella pneumophila* and *Simkania negevensis*, two unrelated bacteria with a wide host range that encode a large and diverse set of DUBs, some of which are highly specific for K6-linked or linear chains.[16–18]

Recently, *Simkania* was found to encode two members of the Josephin family, a somewhat enigmatic DUB class previously thought to be eukaryote-specific.[18] During the characterization of SnJOS1 and SnJOS2, we made the surprising observation that these two enzymes show an unusual cleavage mode: When incubated with ubiquitin chains, both SnJOS1 and SnJOS2 did not cleave the isopeptide bond behind the ubiquitin C terminus but rather the peptide bond between Arg-74 and Gly-75 of ubiquitin. The same bond is also cleaved in mono-ubiquitin, resulting in a non-functional ubiquitin C-terminally shortened by two Gly residues. This activity, which we refer to as ubiquitin C-terminal clippase (UCC), was also observed in many, but not all, additional bacterial Josephin relatives from several bacterial phyla. Their reaction amounts to destructive deubiquitination, since the shortened ubiquitin cannot be re-conjugated, and the diGly remnant left on the substrate lysine precludes further modification of this residue. Eukaryotic Josephins, however, cleave ubiquitin at the canonical DUB position behind Gly-76. By solving the substrate-bound structures of a linkage-promiscuous UCC from *Burkholderia pyrrocinia* (BpJOS) and the closely related conventional DUB from *Pigmentiphaga aceris* (PaJOS), we determined the structural basis of the discordant cleavage positions. Some bacterial UCCs were found to be linkage-specific: the UCC from *Parachlamydia* sp. (PcJOS) cleaved only linear ubiquitin chains, a specificity that could be rationalized through analysis of the PcJOS structure in complex with linear diubiquitin. Taken together, bacterial clippases of the Josephin family allow the bacteria to make deubiquitination an irreversible process.

RESULTS

Simkania Josephins are UCCs

While characterizing the bacterial Josephin-type DUBs from *Simkania negevensis*, we found them inactive against the mono-ubiquitin-based model substrates Ub-AMC and Ub-PA but active against diubiquitin of different linkage types.[18] Since linkage-promiscuous DUBs usually do react with AMC- or PA-based model substrates, we further investigated the chain cleavage mode. SnJOS1 failed to react with a K63-linked diUb-VME probe (Figure S1A), suggesting that the lack of Ub-AMC and Ub-PA reactivity is not due to the absence of the proximal (S1′) ubiquitin moiety. While analyzing K63 diubiquitin cleavage products, we observed masses of ±114 Da in addition to the expected mono-ubiquitin (Figure 1A). This mass difference corresponds to the diGly peptide found at ubiquitin's C terminus, suggesting a cleavage after Arg-74 of both ubiquitin units. Mass-spectrometric analysis of SnJOS1 reaction products using endoproteinase AspN supports this interpretation. As shown in Figure S1B, the spectrum of the peptide DYNIQK$^{(GG)}$ESTLHLVLRLR shows the absence of the C-terminal diGly peptide, while the mass difference between the y11 and y12 fragment ions corresponds to a diGly-modified lysine residue. Cleavage after Arg-74 was also observed when incubating SnJOS1 or SnJOS2 with mono-ubiquitin, resulting in the loss of the terminal diGly (Δ114 Da) from the substrate (Figure S1C). Such a UCC activity has never been observed in physiological enzymes but resembles the ISG15-shortening activity of picornaviral leader peptidase Lb^{pro},[19] engineered to also act on ubiquitin.[20] The diGly remnant on the proximal cleavage product can be detected by a Lys-ε-Gly-Gly antibody (Figure 1B), monitoring the K63-linked Ub_{6+} degradation by SnJOS1/2. Both Simkania clippases show a time-dependent input chain shortening with concomitant Lys-ε-Gly-Gly accumulation on the proximal ubiquitin. To confirm the cleavage position after Arg-74 and address whether Ub-PA's lack of reactivity is due to the unconventional cleavage site, we generated a shortened activity-based probe (Ub$^{1–73}$-PA) replacing Arg-74 with the reactive propargylamine warhead.[21] Both SnJOS1 and SnJOS2 reacted exclusively with Ub$^{1–73}$-PA, not with the conventional Ub$^{1–75}$-PA (Figure 1C), demonstrating that these enzymes react with activity-based probes but require a reactive group at the correct position.

A bacterial Josephin family with different cleavage activities

Eukaryotic Josephins have been consistently described as conventional DUBs,[22–24] with a particular propensity to remove ubiquitin from serine and threonine residues[25] We verified the published results using our assays and found that human ATXN3L and JOSD2 lack clippase activity (Figures S1H and S1I). To investigate whether SnJOS1/2 are exceptional cases or if the shifted cleavage position is a hallmark of a bacterial UCC family, we performed bioinformatical database searches for additional bacterial Josephin homologs.[26] Using generalized profile searches,[27] we identified related sequences in the genomes of several bacteria, including *Burkholderia pyrrocinia* (BpJOS), *Burkholderia catarinensis* (BcJOS), *Pigmentiphaga aceris* (PaJOS), *Herbaspirillum sp.* (HeJOS), and *Parachlamydia*

(E) Analysis of bacterial Josephins cleavage products by western blotting. HEK293T cell lysates were incubated with BpJOS, BcJOS, PaJOS, HeJOS, or PcJOS for 1 h. Substrate deubiquitination and mono-ubiquitin accumulation are shown by α-ubiquitin detection and diGly-remnant accumulation by α-K-ε-GlyGly detection. α-actin staining served as loading control. Asterisks mark unspecific bands.
(F–J) Linkage specificity analysis of bacterial Josephin DUBs. Diubiquitin chains were treated with 50 nM BpJOS (F), 50 nM BcJOS (G), 0.25 μM PaJOS (H), 50 nM PcJOS (I), or 2.5 μM HeJOS (J) for indicated times.
(K) Intact mass spectrometry of M1-linked diubiquitin cleaved by PcJOS. The x axis shows *m/z* ratio, with deconvoluted masses next to peaks. Input sample shows a 17,100 Da peak (green) corresponding to diubiquitin, cleaved by PcJOS to three products (blue) corresponding to ubiquitin (8,558.6) or ubiquitin ±diGly peptide (8,672/8,444 Da).
See also Figures S1 and S2 and Table S1.

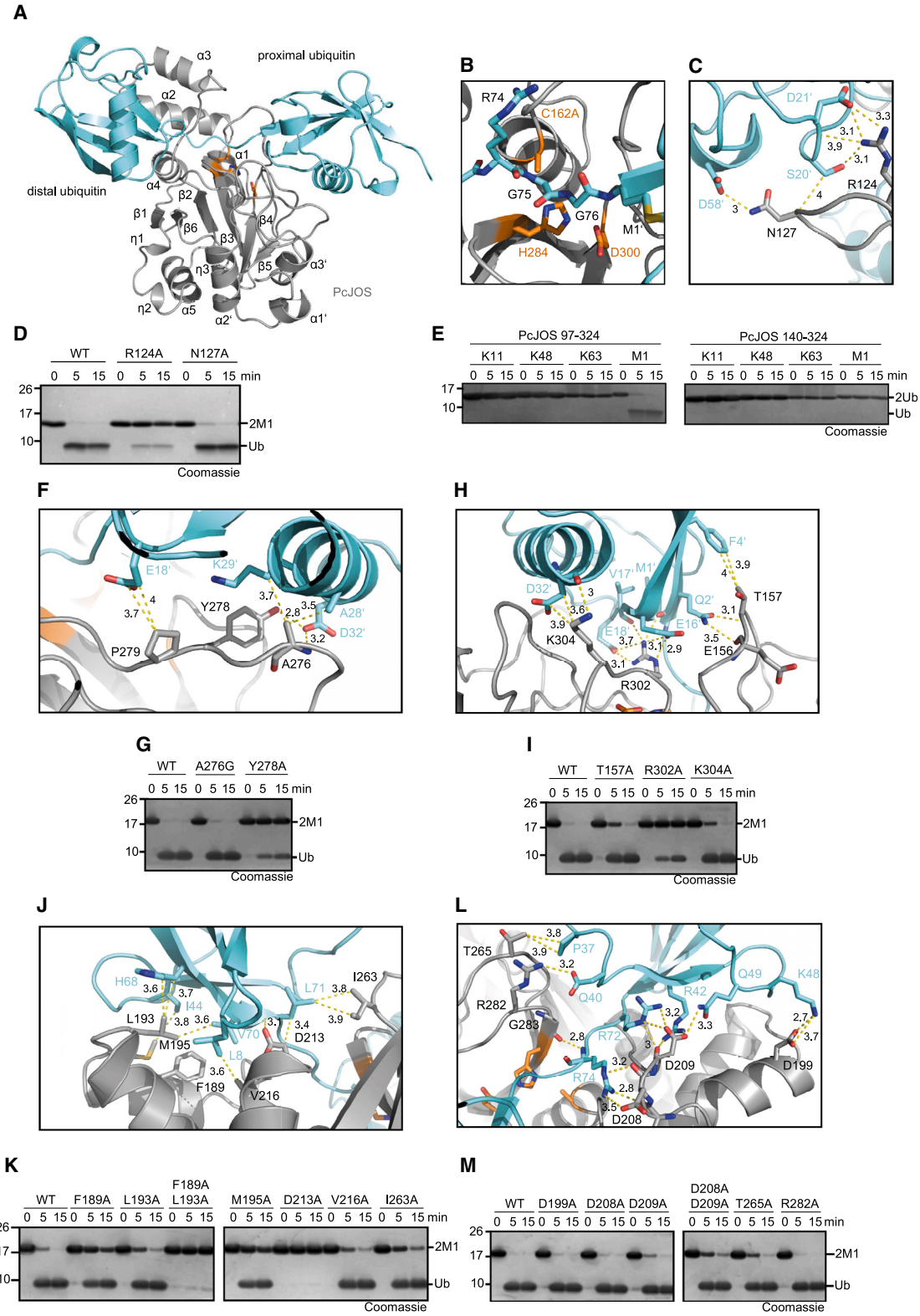

Figure 2. Crystal structure of PcJOS with linear diubiquitin

(A) Overview of the complex in cartoon representation. The catalytic core of PcJOS is gray, and ubiquitin is light blue. Catalytic residues are shown as orange sticks.

(legend continued on next page)

sp. (PcJOS) (Figure S2A). We expressed the predicted catalytic domains of these enzymes in *E. coli*, purified them, and characterized their catalytic properties. The *Burkholderia* Josephins BpJOS and BcJOS reacted only with the truncated Ub^{1-73}-PA probe, suggesting a clippase activity. By contrast, *Pigmentiphaga* PaJOS reacted exclusively with the conventional Ub^{1-75}-PA probe, indicating that UCC activity is not a general feature of the bacterial Josephin family (Figure 1D). The cleavage positions were confirmed using intact mass spectrometry (MS) (Figures S1D–S1F). The two remaining candidates, HeJOS and PcJOS, reacted with neither probe, suggesting that they are inactive or require a particular linkage type for their activity (Figure 1D). When incubating the purified enzymes with HEK293 cell lysate and visualizing the products with ubiquitin- or Lys-ε-diGly-directed antibodies, the results supported the probe reactivity data (Figure 1E). BpJOS and BcJOS completely deconjugated all cellular ubiquitin and left diGly remnants on their substrates. In line with the probe results, PaJOS did not generate diGly remnants, although some ubiquitin was de-conjugated. HeJOS appeared similar to PaJOS, with no diGly production but a modest reduction in high-molecular-weight (MW) chains. PcJOS appeared inactive in this experiment, as neither chain reduction nor antibody-detectable diGly remnants were observed (Figure 1E).

Linkage specificity was analyzed using a panel of differently linked diubiquitins. The Burkholderia clippases BpJOS and BcJOS cleaved all chain types within minutes, with the exception of K27-linked diubiquitin, which was only poorly cleaved (Figures 1F and 1G). By contrast, the conventional DUB PaJOS was highly specific for K63-linked chains, highlighting the differences within the bacterial JOS family (Figure 1H). HeJOS and PcJOS, which were inactive against activity-based probes, specifically cleaved K63- or M1-linked chains, respectively (Figures 1I and 1J). To determine the cleavage position of the linkage-specific Josephins, the proteases were incubated with the respective diubiquitin species, and the generated mono-Ub was analyzed using intact MS. The HeJOS-generated ubiquitin had a mass of 8,558.6 Da, indicating conventional DUB cleavage (Figure S1G). In the case of PcJOS, the cleaved linear diubiquitin showed masses of 8,444.6, 8,558.6, and 8,672.6 Da, indicating that the C-terminal diGly was cleaved off the distal ubiquitin and remained attached to the N terminus of the proximal ubiquitin (Figure 1K). The free C terminus of the proximal ubiquitin was poorly clipped, underscoring the requirement of an M1-linkage for PcJOS activity.

The activity of BpJOS as a linkage-promiscuous clippase is reminiscent of Lb^{pro*}, a variant of the viral leader peptidase Lb^{pro} engineered to also function on ubiquitin chains, which are cleaved without linkage selectivity.[20] We compared the activity of BpJOS and Lb^{pro} toward ubiquitin and ubiquitin-like modifiers. While Lb^{pro*} reacted with the clippase probes Ub^{1-73}-PA, $NEDD8^{1-73}$-PA, and $ISG15^{79-154}$-PA, BpJOS only reacted with ubiquitin and NEDD8 probes (Figure S2B). The inactivity of BpJOS toward ISG15 was confirmed by intact MS (Figure S2C). By contrast, the activity of BpJOS toward K48-linked diubiquitin exceeded that of Lb^{pro*} by several orders of magnitude (Figure S2D).

Structural basis of M1-specific ubiquitin clipping by PcJOS

To understand the structural basis of the shifted UCC cleavage site in a linkage-specific context, we determined the structure of PcJOS in complex with its substrate. The catalytic fragment $PcJOS^{70-324}$, rendered inactive through mutation of the predicted active site residue Cys-162 to alanine (Figure S2A), was crystallized with linear diubiquitin, and the crystal structure was solved to a resolution of 2.18 Å. The asymmetric unit contained one diubiquitin molecule bound by two PcJOS molecules, the first bound between the ubiquitin units, and the second bound to the C terminus of the diubiquitin (Figure S3A). In the first $PcJOS^{70-324}$ molecule (chain A), region 97–324 was fully resolved, and chain C showed a nearly identical conformation with a root-mean-square deviation (RMSD) of 0.44 Å over 1,317 atoms (Figure S3B). The PcJOS catalytic domain comprises a papain-fold core domain reminiscent of other Josephin-type DUBs (α1-β6) and an N-terminal extension formed by helices α1′-α3′ (Figure 2A). The active site consists of Cys-162 (Ala-162 in the structure), His-284, and Asp-300, in line with the alignment-based prediction (Figure S2A). In the first PcJOS molecule, the active site is placed next to the scissile peptide bond between Arg-74 and Gly-75 of the distal (S1) ubiquitin, compatible with the observed clippase activity (Figure 2B).

(B) Magnification of the PcJOS active site. Important residues are orange (PcJOS active site) or light blue (ubiquitin C terminus) sticks. The position of the ubiquitin C terminus confirms cleavage between Arg-74 and Gly-75.
(C) The N-terminal extension is part of the S1′ ubiquitin-binding site. Key residues are light blue (ubiquitin) or gray (PcJOS) sticks. Hydrogen bonds are shown as dotted lines.
(D) Activity of PcJOS R124A or N127A against linear diubiquitin.
(E) Activity of PcJOS truncations against differently linked diubiquitins.
(F) Tyr-278 is critical in the S1′ ubiquitin-binding site. Tyr-278 and neighboring residues are light blue (ubiquitin) or gray (PcJOS) sticks. Key interactions are shown as dotted lines.
(G) Activity of PcJOS A276A or Y278A against linear diubiquitin.
(H) Extensive contacts between PcJOS catalytic core and proximal ubiquitin. Key residues are light blue (ubiquitin) or gray (PcJOS) sticks. Interactions are indicated by dotted lines.
(I) Activity of wild-type PcJOS and S1′ site mutants (T157A, R302A, and K304A) against linear diubiquitin.
(J) The α2/α3 region is part of the S1 site and recognizes the hydrophobic Ile-44 patch of distal ubiquitin. Residues involved are light blue (ubiquitin) or gray (PcJOS) sticks. Hydrophobic interactions are shown as dotted lines.
(K) Activity of S1 site mutants against linear diubiquitin.
(L) The C terminus of distal ubiquitin is stabilized by polar interactions. Residues involved are light blue (ubiquitin) or gray (PcJOS) sticks.
(M) Mutational analysis of residues stabilizing ubiquitin's C terminus.
See also Figure S3 and Table S2.

Mutation of any active site residue to alanine resulted in a complete loss of cleavage activity (Figure S3C). Structural database searches using DALI[28] yielded several Josephin DUBs as the best matches, including human JOSD2 (PDB: 6PGV)[24] and ATXN3L (PDB: 3O65),[22] thus supporting the assignment of PcJOS to the Josephin family. The structural similarity was most pronounced within the catalytic core region (Figure S3D), including the active site residues (Figure S3E), and structural superposition of the core region resulted in RMSDs of 1.4 Å over 500 atoms for JOSD2 and 3.7 Å over 574 atoms for ATXN3L. Two striking differences between PcJOS and eukaryotic Josephins are the extended N-terminal helix bundle ($\alpha1'$-$\alpha3'$, residues 97–140) and major conformational differences in helices $\alpha2/\alpha3$ (residues 178–208). The $\alpha2$ helix is shorter than that in ATXN3L, causing the $\alpha3$ helix to shift. In the available JOSD2 structure, the corresponding region is not resolved. Interestingly, these regions make important contacts with the proximal (S1′) and distal (S1) ubiquitin units, respectively.

The S1′ ubiquitin forms an extensive hydrogen-bond network with PcJOS (chain A). Within the N-terminal extension, Arg-124 and Asn-127 form hydrogen bonds with Ser-20′/Asp-21′ and Asp-58′ of the proximal ubiquitin, respectively (Figure 2C). The former contacts are important, since the R124A mutant lost activity almost completely, while N127A did not affect the activity (Figure 2D). To investigate whether the N-terminal region causes M1-linkage specificity by sterically inhibiting other chain types, we tested a truncated version of PcJOS that lacks this region but contains all the structural elements considered important for Josephin catalysis. Unlike the slightly truncated PcJOS$^{97–304}$, which maintained M1-specific cleavage, truncated PcJOS$^{140–304}$ lacking the N-terminal extension was inactive against all tested diubiquitin species and activity-based probes (Figures 2E and S3F). Thus, the M1 specificity of PcJOS is unlikely to be due to the blocking of other chain types but rather induced by specific linear chain recognition or substrate-assisted catalysis. Additional S1′ contacts are made by loop 275–278, where Tyr-278 contributes a hydrogen bond to Asp-32′, while Ala-276 shows hydrophobic interactions to Ala-28′ and Lys-29′ of the proximal ubiquitin (Figure 2F). As shown in Figure 2G, the Y278A mutant was nearly inactive, while the A28G mutation did not affect activity, suggesting that the Tyr-278 contact is more important for S1′ recognition. In addition, several residues outside this loop contact the proximal ubiquitin (Figure 2H). Arg-302 shows extensive hydrogen bonding with the Glu-16′ and Glu-18′ sidechains and with main-chain atoms of Val-17′ and Met-1′. Lys-304 forms a hydrogen bond with the ubiquitin main chain at Asp-32′, and Thr-157 is packed against Phe-4′ of the proximal ubiquitin. Among these contacts, Arg-302 appears to be most important, since the R302A mutant was almost inactive, whereas the K304A and T157A mutants reduced activity only marginally (Figure 2I). To assess whether the side-chain contacts of Arg-302 to Glu-16′ and Glu-18′ are both important, wild-type PcJOS was tested against diubiquitin carrying the point mutants E16'A or E18'A. As shown in Figure S3G, neither mutant was cleaved, indicating that both hydrogen bonds are required. Overall, the proximal ubiquitin appears to be positioned in a cleavable conformation by a multitude of distinct interactions.

Interactions at the S1 position include recognition of the hydrophobic Ile44-patch by the $\alpha2/\alpha3$ region and several polar interactions at the C terminus of ubiquitin close to the scissile bond. Ubiquitin Ile-44 itself contacts Met-195 of PcJOS, whereas the residues surrounding the patch (Val-70, His-68, and Leu-8) show hydrophobic interactions with Leu-193, Val-216, and Phe-189 of PcJOS (Figure 2J). Abrogating these interactions individually by the mutations M195A, L193A, V216A, or F189A modestly reduced the activity, whereas the double-mutant F189A/L193A was completely inactive (Figure 2K). An additional hydrogen bond between Asp-213 and the main chain of Leu-71 also appeared to be crucial, since the D213A mutant was inactive (Figures 2J and 2K). Most DUBs recognize and position the cleavable ubiquitin C terminus through salt bridges and/or hydrogen bonds between Arg-72 and Arg-74 of ubiquitin and acidic or otherwise polar residues of the enzyme. In the PcJOS structure, Arg-72 and Arg-74 contact Asp-209 and Asp-208, respectively (Figure 2L). However, mutations in these residues (D208A, D209A, and D208A/D209A) only marginally reduced diubiquitin cleavage (Figure 2M). In contrast to other DUBs, Arg-72 and Arg-74 not only bind to the side-chain carboxyl groups of Asp-208/Asp-209 but also to their main-chain carbonyls, which are not affected by mutagenesis. This explanation is supported by experiments using R72A and R74A mutated ubiquitin substrates, which are mostly inert to PcJOS cleavage, demonstrating the importance of these two arginine residues for activity (Figure S3G). Additional interactions were observed between Arg-282 and ubiquitin Gln-40 and between Thr-265 and ubiquitin Pro-37 but do not appear crucial since the mutants T265A and R282A were nearly as active as wild-type PcJOS. In DUBs with conventional cleavage mode, the catalytic histidine residue is usually followed by an aromatic "gatekeeper" residue, which interacts with Gly-75 and—among other functions—restricts active site access of substrates without small amino acids at this position.[17] In UCCs, which cleave after Arg-74, such a gatekeeper role should not be required. Nevertheless, many clippases identified in this study do conserve the aromatic residue (Figure S2A). In PcJOS, the catalytic His-284 is followed by Phe-285, which contacts Leu-73, the residue preceding Arg-74, after which cleavage occurs (Figure S3H). To investigate the importance of this interaction, we tested mutations of the "gatekeeper residue" and its interaction partner. As shown in Figures S3G and S3I, the activity of the F285A mutant was abolished, and the L73A-mutated ubiquitin was completely resistant to cleavage.

Structural determinants for clippase-type cleavage

The bacterial Josephin family contains both clippases and conventional DUBs, which raises the question of how the cleavage position is determined. Of particular interest are the family members BpJOS (UCC) from *Burkholderia pyrrocinia* and PaJOS (DUB) from *Pigmentiphaga aceris* since they are closely related yet differ in their cleavage modes. For conventionally cleaving PaJOS, the catalytic fragment PaJOS$^{2–265}$ was crystallized in a covalent complex with Ub-PA. The structure was solved at a resolution of 1.89 Å with an asymmetric unit containing twelve PaJOS/Ub complexes, which were nearly identical with RMSDs ranging from 0.1 to 0.3 Å. Overall, the structure revealed

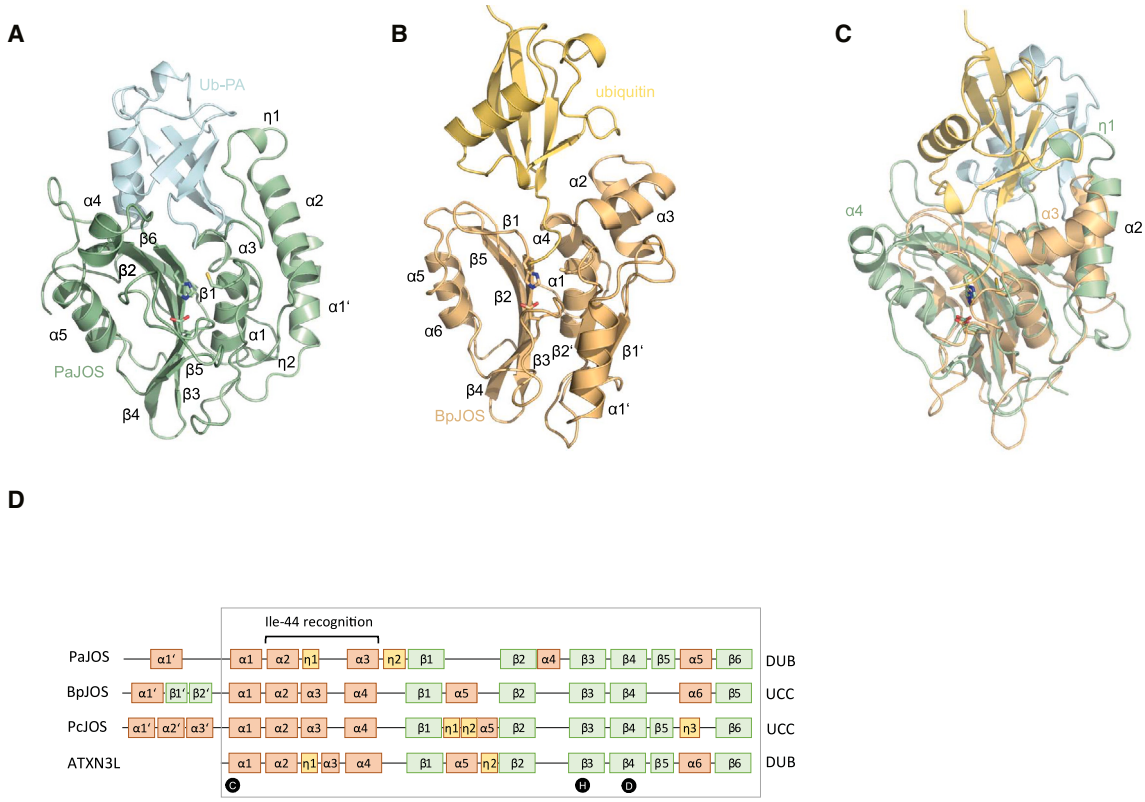

Figure 3. Crystal structures of PaJOS and BpJOS in complex with ubiquitin

(A) Overview of the PaJOS/Ub-PA complex in cartoon representation. The catalytic core of PaJOS is in green and ubiquitin in light blue. The catalytic residues are shown as sticks.

(B) Overview of the BpJOS/ubiquitin complex in cartoon representation. The catalytic core of BpJOS is colored orange and ubiquitin is yellow. The catalytic residues are shown as sticks.

(C) Structural superposition of the DUB PaJOS and the UCC BpJOS structures shown in (A and B). The superposition is based on the catalytic domains, which align with an RMSD of 1.29 Å over 522 atoms. Secondary structure elements differing in the structures are numbered.

(D) Schematic overview of secondary structure elements of bacterial Josephins compared with human ATXN3L. The catalytic core domain is indicated by a gray box. The position of the catalytic residues is marked by black circles.

See also Table S3.

a Josephin-like papain fold (α1-β6) with an N-terminal extension of a single helix α1′ (Figure 3A). The active site residues were determined as Cys-66, His-187, and Asp-203, confirming their sequence-based prediction. Mutating any of the active site residues to alanine caused a loss of cleavage activity (Figures S4A and S4B). For the promiscuous clippase BpJOS, the catalytically inactivated full-length protein BpJOS^{C69A} was crystallized in complex with linear diubiquitin. The structure was solved at a resolution of 2.56 Å. The asymmetric unit contained two BpJOS/ubiquitin complexes, each of which contained only one ubiquitin moiety at the S1 position (Figure S4C). The electron density suggested that the visible S1-bound ubiquitin corresponds to the C-terminal unit of the diubiquitin substrate, while the N-terminal unit is disordered owing to the lack of a defined interface. In both BpJOS chains, residues 15–218 were resolved, and their conformation was nearly identical with an RMSD of 0.2 Å over 1,308 atoms (Figure S4D). The resolved region corresponds to the minimal active fragment of BpJOS, since further truncation of the N-terminal α-helix and the first two β-strands, which are not conserved in PaJOS, caused a complete loss of activity (Figure S4E). Overall, the BpJOS structure revealed a Josephin-like papain fold with a core (α1-β5) similar to PaJOS, preceded by a unique N terminus consisting of one helix and two β-strands (α1′-β2′) (Figure 3B). The active site residues were identified as Cys-69 (Ala-69 in the structure), His-166, and Asp-182, and their individual replacement by alanine universally abolished activity (Figures S4F and S4G).

In accordance with their sequence similarity, the catalytic domains of PaJOS and BpJOS can be superimposed with an RMSD of 1.29 Å over 522 atoms (Figure 3C). However, the bound S1 ubiquitin molecules do not superimpose, since they are bound in a different orientation, which ultimately causes displacement of their C termini and thus a shifted cleavage position. The differences in ubiquitin binding appear to be caused by subtle changes in protease structure. Both enzymes bind the Ile-44 patch of S1-ubiquitin through homologous regions corresponding to α2/η1/α3 in PaJOS and α2/α3/α4 in BpJOS (Figure 3D), with poorly conserved sequences and major structural

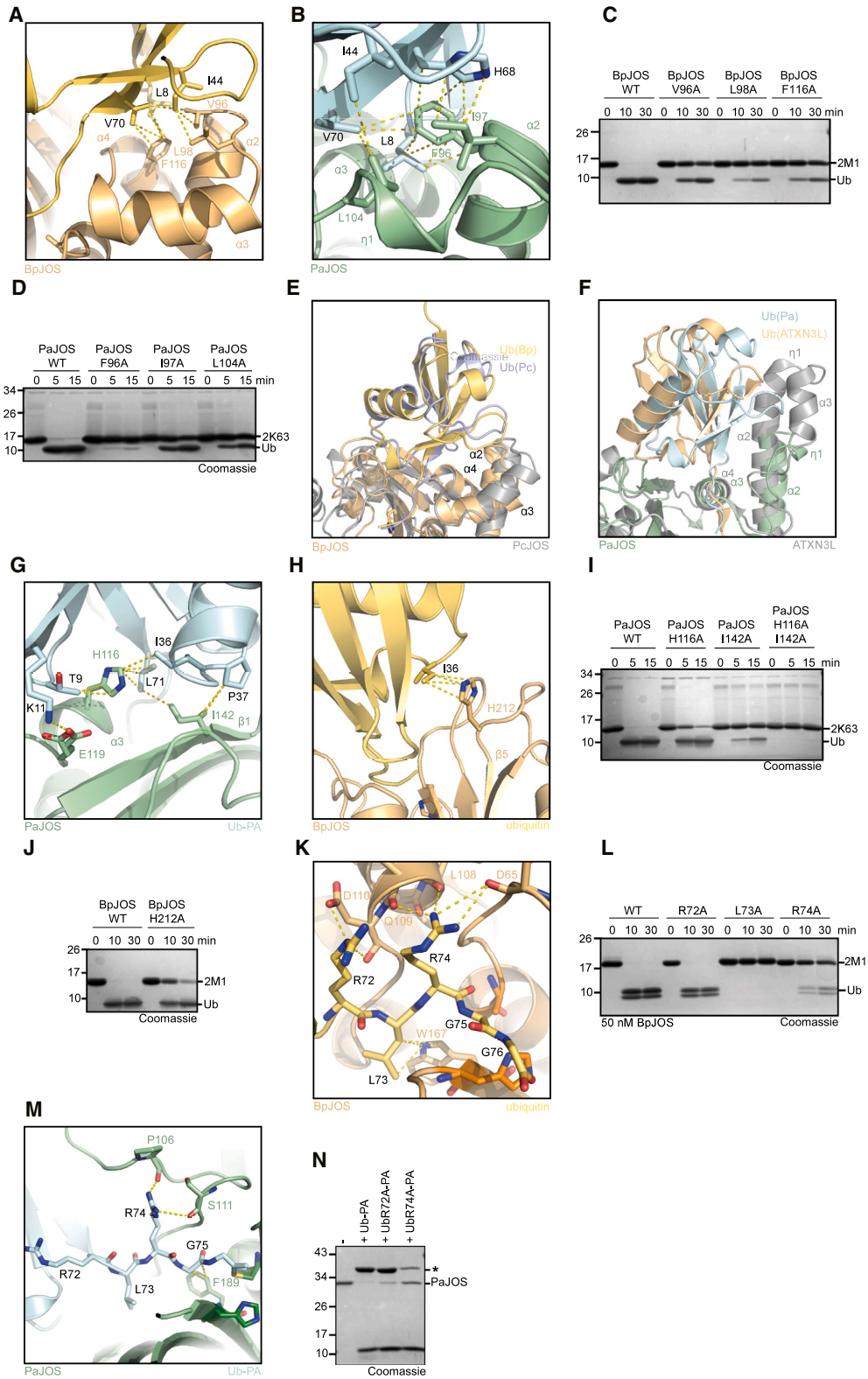

Figure 4. Differential S1 ubiquitin binding by Josephin family DUBs and UCCs

(A) Recognition of ubiquitin's Ile-44 patch by BpJOS α2/α3/α4 region. Residues involved are highlighted as yellow (ubiquitin) or light orange (BpJOS) sticks. Hydrophobic interactions are indicated by dotted lines.

(legend continued on next page)

differences. In BpJOS, this region forms a rigid helical structure and contacts the Ile-44 patch via Val-96, Leu-98, and Phe-116 (Figure 4A). Here, the α3 helix provides rigidity but does not directly contact ubiquitin. By contrast, the corresponding region of PaJOS is more flexible, and α2 is extended by the short helix η1 and connected via an unstructured loop to α3. The ubiquitin Ile-44 patch is contacted by Phe-96, Ile-97, and Leu-104 (Figure 4B). Mutagenesis of these hydrophobic residues showed that for both enzymes, ubiquitin cleavage is highly dependent on these contacts (Figures 4C and 4D). The structural differences in the Ile-44 recognition regions are likely to cause the different orientation of the bound ubiquitin. Among other steric problems, the S1 ubiquitin bound by BpJOS would clash with η1 of PAC.

To investigate if the two ubiquitin-binding modes are conserved in other Josephin UCCs and DUBs, we compared the two available clippase structures BpJOS and PcJOS, whose catalytic domains can be superimposed with an RMSD of 2.36A over 619 atoms. As shown in Figure 4E, the position of the α3 helices of BpJOS and PcJOS are conserved, and the orientation of the bound ubiquitin is nearly identical (Figure 4E). Conversely, both the conventionally cleaving PaJOS and the eukaryotic DUB ATXN3L use their α2 helices, each of them extended by a short η1 helix, to position the S1 ubiquitin ready for DUB cleavage (Figure 4F). Taken together, the available data suggest that Josephin-type UCCs use the helices following the catalytic cysteine in a conserved way to position the S1 ubiquitin for clippase cleavage, while bacterial Josephin-type DUBs resemble their eukaryotic counterparts. Both PaJOS and BpJOS have a second ubiquitin-binding interface contacting the Ile-36 patch. In PaJOS, residues His-116 and Ile-142 engage in hydrophobic interactions with Thr-9, Ile-36, Pro-37, and Leu-71 of the S1 ubiquitin (Figure 4G). In BpJOS, His-212 interacts with Ile-36 of ubiquitin (Figure 4H). In both cases, these interactions are important for full activity, as demonstrated by mutational analysis (Figures 4I and 4J). Owing to the different ubiquitin orientations, Ile-36 recognition involves different regions of PaJOS and BpJOS (Figure S4H). While the DUB-typical Ile-36 recognition is conserved between PaJOS and ATXN3L (Figure S4I), the recognition in UCC orientation differs between the two available clippase structures. The loop, which in BpJOS contacts Ile-36, is shorter in PcJOS. Instead, Ile-263 from a neighboring loop contacts Leu-71 in ubiquitin. Despite their different sequence positions, the contact residues occupy a similar space, resulting in a conserved orientation of the bound ubiquitin (Figure S4J).

Since UCCs bind the ubiquitin C terminus shifted by two residues relative to DUBs, major differences in positioning the ubiquitin tail are expected. In PcJOS, Arg-72 and Arg-74 are crucially stabilized by hydrogen bonds with backbone atoms (Figures 2L and S3G), and an analogous binding mode was observed for BpJOS. Arg-74 of ubiquitin, the residue directly preceding the scissile bond, forms strong hydrogen bonds with backbone atoms of Asp-65, Leu-108, and Gln-109 of BpJOS. Another hydrogen bond was observed between Arg-72 of ubiquitin and Asp-110 of BpJOS (Figure 4K). Accordingly, linear R74A diubiquitin was hardly cleaved by BpJOS, whereas the R72A substitution had no visible effect on cleavage (Figure 4L). Leu-73, the hydrophobic residue between Arg-72 and Arg-74, contacts Trp-167 of BpJOS (and Phe-285 of PcJOS) and is crucial for catalysis (Figures 4K and 4L). In the conventionally cleaving and K63-preferring PaJOS, Arg-74 of ubiquitin is also stabilized by a main-chain hydrogen bond, albeit to a different region of the protease (Pro-106 and Ser-111). Arg-72 does not show strong interactions (Figure 4M). Accordingly, PaJOS reacted with R72A-PA, whereas its reaction with R74A-PA was strongly impaired (Figure 4N). Unlike BpJOS, PaJOS does not interact with Leu-73, which appears to be a clippase-specific requirement. Instead, the aromatic gatekeeper residue Phe-188 stabilizes Gly-75, as is commonly observed in conventional DUBs (Figure 4M). The effect of the F188A mutant on diubiquitin cleavage was modest (Figure S4K). The shifted ubiquitin C terminus is shown in Figure S4L, which highlights that although both require stabilization of R74, the interacting residues are located differently.

The different ubiquitin-binding modes of UCCs and conventional DUBs raise the question of whether the cleavage type can be altered by exchanging the respective ubiquitin-recognition regions. Assuming that the Ile44 patch recognition through α2/α3 of clippases and α2/η1 of DUBs is the most crucial determinant, these regions were swapped between BpJOS and PaJOS to create chimeric enzymes (Figure S5A). However, when trying to convert the DUB PaJOS to a clippase by replacing residues 82–112 with 84–110 of BpJOS, no folded protein was

(B) Recognition of ubiquitin's Ile-44 patch by PaJOS α2/η1/α3 region. Residues involved are highlighted as light blue (ubiquitin) or green (PaJOS) sticks. Hydrophobic interactions are indicated by dotted lines.
(C) Activity of wild-type BpJOS or S1 site mutants against linear diubiquitin.
(D) Activity of wild-type PaJOS or S1 site mutants against K63-linked diubiquitin.
(E) Structural superposition of UCCs BpJOS (orange) and PcJOS (gray). Superposition based on catalytic domains aligning with an RMSD of 2.362 Å over 619 atoms. Bound ubiquitin molecules are in almost identical orientation, and conserved secondary structure elements involved in ubiquitin binding are numbered.
(F) Structural superposition of DUBs PaJOS (green) and ATXN3L (gray, PDB: 3O65), based on catalytic domains aligning with an RMSD of 2.37 over 520 atoms. Bound ubiquitin molecules are in similar orientation, and secondary structure elements involved in binding are numbered.
(G and H) Ile36-patch recognition by PaJOS (G) or BpJOS (H). Residues involved are highlighted as sticks.
(I) Activity of wild-type PaJOS or S1 site mutants against K63-linked diubiquitin.
(J) Activity of wild-type BpJOS or H212A against linear diubiquitin.
(K) Recognition of ubiquitin's C terminus by BpJOS. Residues involved are highlighted as yellow (ubiquitin) or light orange (BpJOS) sticks. Important interactions are indicated by dotted lines.
(L) Activity of BpJOS against ubiquitin mutants. N-terminally His-tagged and mutated linear diubiquitin was incubated with BpJOS for indicated time points.
(M) Recognition of ubiquitin's C terminus by PaJOS. Residues involved are highlighted as light blue (ubiquitin) or green (PaJOS) sticks. Important interactions are indicated by dotted lines.
(N) Activity-based probe reaction of PaJOS with wild-type, R72A, or R74A Ub1-75-PA. Reaction was stopped after 3 h.
See also Figure S4.

obtained. Conversely, when replacing 84–110 of BpJOS with 82–112 of PaJOS, the chimeric protein dBpJOS could be purified but was enzymatically inactive (Figures S5B and S5C). Assuming that Ile-36 patch recognition might also be important and the swapped helices might need specific support from the rest of the structure, the swapped regions were reduced to maintain more of their original support structure. Because PaJOS lacks a structural scaffold to engineer clippase-type Ile36 recognition, the second chimeric construct focused on converting BpJOS into a normal DUB. The last two residues of α2 and the complete α3 of BpJOS were replaced by the corresponding regions of PaJOS. In addition, Asn-115 was mutated to His to create a DUB-like contact for Leu-8 of ubiquitin, His-212 was mutated to Ala to remove the UCC-like recognition of Ile-36, and Ala-134 was mutated to Ile to introduce a DUB-like binding of the Ile-36 patch (Figures S5D–S5F). However, the resulting dBpJOS-II chimera was still completely inactive (Figures S5G and S5H). We reasoned that another problem might be insufficient stabilization of the ubiquitin C terminus in the chimera. The clippase BpJOS specifically recognizes Arg-74, but not Arg-72, of the S1 ubiquitin. After engineering BpJOS to a conventional DUB, Arg-74 would occupy the position of Arg-72 and not be stabilized. To address this problem, we generated an AlphaFold model of the chimera dBpJOS-II in complex with ubiquitin (Figure S5I) and designed a number of (single) mutations (G76D, G76E, A110D, or A110E) that might stabilize Arg-74 in DUB mode. However, none of the chimeras generated showed any activity (Figures S5J and S5K). Thus, it appears that exchanging UCC and DUB activities is not straightforward and might require an extensive redesign of the ubiquitin-binding surfaces and their support structure.

Predictability of the cleavage position

Among the bacterial Josephins described are four linkage-promiscuous UCCs, one M1-specific UCC, and two conventionally cleaving DUBs. To expand knowledge of clippases, search for additional linkage-specificities, and test if structural modeling can predict cleavage mode, we performed a comprehensive bioinformatical search for candidates. We selected eight representative proteins for experimental validation (PtJOS, KrJOS, MtJOS, MxJOS, ScJOS, MlJOS, Pc2JOS, and CsJOS; see Table S1 for accession data and Figure S2A for alignment). By subjecting the catalytic domains to AlphaFold modeling in complex with ubiquitin, seven plausible models were obtained (Data File S1). KrJOS yielded an unsatisfactory model with poor complex confidence score (iptm + ptm < 0.35). A superposition of the resulting models with the ubiquitin-bound structures of a clippase (BpJOS) and a DUB (PaJOS) revealed that only MxJOS had ubiquitin in the DUB-typical arrangement, whereas the other six models showed a clippase-oriented S1 ubiquitin (Figures 5A and S6).

For all eight candidates, the catalytic domains were expressed in *E. coli*, purified, and tested for cleavage mode and possible linkage specificity. KrJos, the candidate without a convincing AlphaFold model, was poorly expressed and did not react with the UCC-specific probe Ub^{1-73}-PA or with the DUB-specific Ub^{1-75}-PA (Figure 5B). For candidates with high-confidence complex models, the experimentally determined cleavage modes matched structure-based predictions: MxJOS reacted only with conventional Ub^{1-75}-PA, whereas MtJOS, PtJOS, ScJOS, MlJOS, and Pc2JOS reacted only with the clippase probe Ub^{1-73}-PA (Figure 5B). All these enzymes cleaved diubiquitin species of various linkage types without much selectivity (Figures 5C–5I). By contrast, CsJOS from *Chlamydiales bacterium ST3* did not react with any probes and exclusively cleaved linear diubiquitin (Figures 5B and 5J). Since linkage-specific DUBs often do not react with probes, we analyzed the M1-linked diubiquitin digestion by intact MS and found that CsJOS cleaves in clippase mode, as predicted from the structural model (Figure 5K).

DISCUSSION

Intracellular bacteria use a variety of effectors to counteract host ubiquitin-based defense mechanisms. Besides DUBs, which can reverse the action of host E3 ligases,[11] effector types have been described that can prevent access of ligases to bacteria,[9] methylate bacterial surface lysines,[29] impair host ubiquitin through deamidation,[10] or destroy host E2 enzymes by cross-linking them to ubiquitin.[30] UCCs are additional weapons in the bacterial armory that combine the deubiquitination of undesirable targets with the irreversible destruction of the modifier and the protection of the modification site against re-modification. We identified Josephin-type clippases in diverse bacterial phyla, including Pseudomonadota, Chlamydiota, Myxococcota, Acidobacteriota, and Cyanobacteria (Table S1), but their occurrence within these phyla is restricted to a few species, excluding the major human pathogens. At first glance, clippase effectors appear ideal for bacterial subversion of the host ubiquitin-based defense, which raises the question of why not more bacteria use clippases rather than conventional DUBs. One possible explanation is that many bacteria rely on ubiquitin ligase activity, which would make the wholesale destruction of ubiquitin disadvantageous. Moreover, high clippase activity maintained over a longer period may be cytotoxic by depleting functional ubiquitin and/or clogging ubiquitin-recognition components through dysfunctional truncated ubiquitin. Among the clippase-encoding bacteria, only *Simkania negevensis* has been shown to infect human cells,[31] but the expression levels of SnJOS1 and SnJOS2 during infection are very low,[18] and both enzymes have rather modest activities (Figure 1B). At the other end of the spectrum is the highly active BpJOS from *Burkholderia pyrrocinia*, a bacterium that is occasionally found in cystic fibrosis patients but lacks an infection model.[32]

Bacterial Josephin-family clippases are the only naturally occurring enzymes with ubiquitin-directed clipping (UCC) activity. The leader peptidase Lb^{pro} of foot-and-mouth disease virus (FMDV) cleaves, besides the viral polyprotein, the ubiquitin-like modifier ISG15 before the terminal GlyGly.[19] Based on Lb^{pro}, a variant enzyme, Lb^{pro*}, has been engineered to show reduced modifier specificity, including ubiquitin and NEDD8.[20] However, its UCC activity remains several orders of magnitude lower than that of BpJOS (Figure S2D). Unlike the singleton Lb^{pro}, bacterial clippases belong to an extended family that contains both UCC and DUB members. These favorable circumstances allowed us to address the structural changes required to shift the cleavage

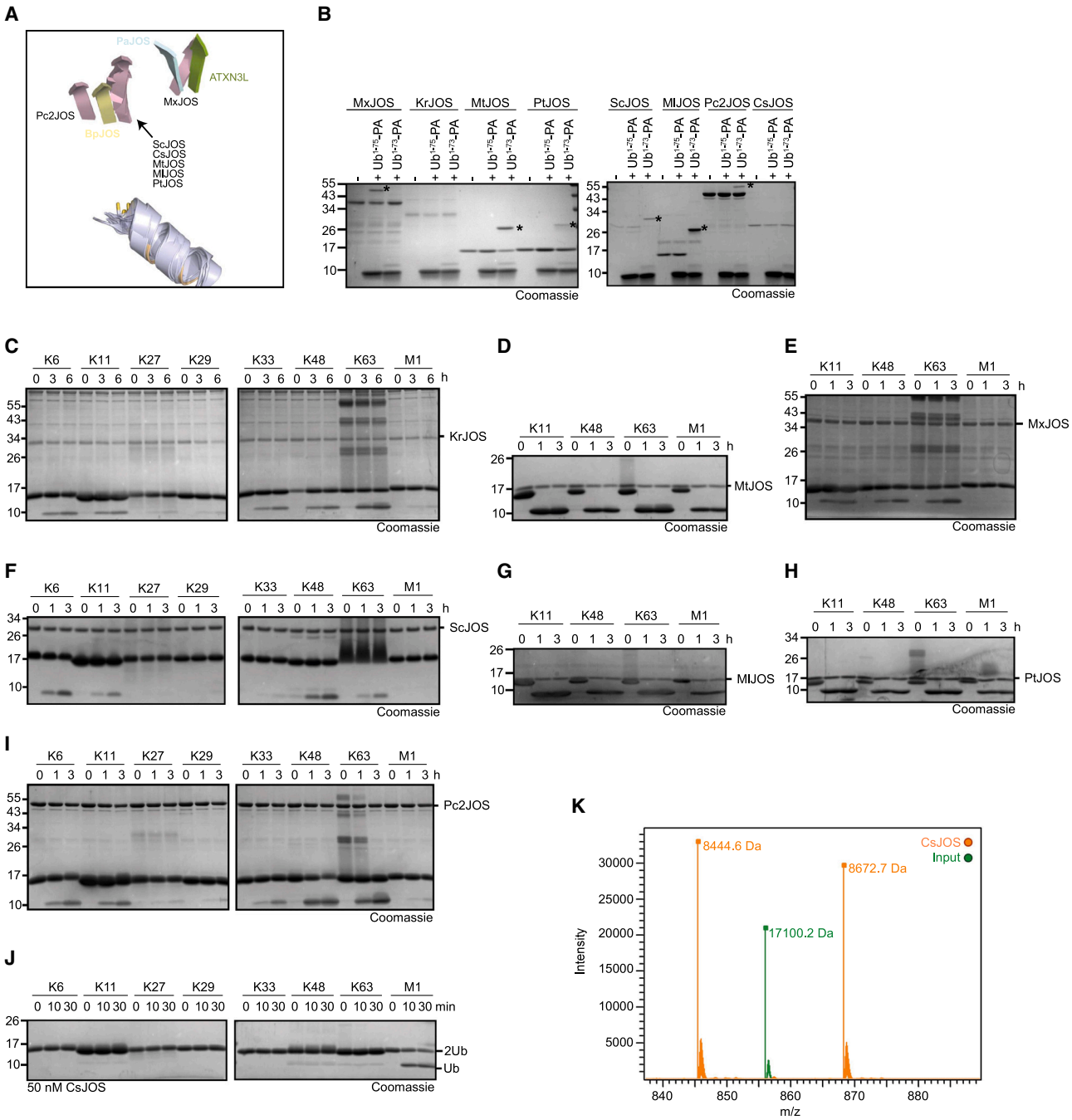

Figure 5. Predictability of UCC and DUB cleavage

(A) Structures of divergent bacterical Josephins were predicted using AlphaFold2 in complex with ubiquitin. The models and crystal structures of BpJOS and ATXN3L (PDB: 3O65) were superimposed onto PaJOS. For each model, only the catalytic cysteine-containing helix and β-3 of the bound ubiquitin are shown. Comparison of the relative orientation of the bound ubiquitin β-strand (pink) to PaJOS (light blue)/ATXN3L (green) or BpJOS (yellow) allows predicting DUB or clippase activity.

(B) Determination of cleavage position by activity-based probes. New candidates shown in (A) were incubated with $Ub^{1–75}$ or $Ub^{1–73}$-PA probes for 18 h. Asterisks mark shifted bands after reaction.

(C–J) Linkage specificity analysis of bacterial Josephin DUBs. Diubiquitin chains were treated with 10 μM KrJOS (C), 5 μM MtJOS (D), 5 μM MxJOS (E), 5 μM ScJOS (F), 5 μM MlJOS (G), 5 μM PtJOS (H), 5 μM Pc2JOS (I), or 50 nM CsJOS (J) for indicated time points.

(K) Intact mass spectrometry of M1-linked diubiquitin cleaved by CsJOS. The *m/z* ratio is on the x axis with deconvoluted masses shown next to respective peaks. The input sample shows a single 17,100 Da peak (green) corresponding to diubiquitin's monoisotopic mass, cleaved by CsJOS to two products (blue) corresponding to ubiquitin's monoisotopic mass ± a GlyGly peptide (8,672/8,444 Da).

See also Figure S6 and Table S1.

site by two positions. At least within the Josephin family, the crucial factor is the orientation of the bound S1 ubiquitin, whose Ile-44 patch is recognized by the variable α2/α3/α4 region located between the helix (α1) and the first β-strand of the papain fold (Figure 3). The available UCC and DUB structures differ markedly within this region, resulting in clearly distinct ubiquitin orientations. Interestingly, the α2/α3/α4 region shows considerable variability among different clippases, both in sequence and (predicted) structure, while the orientation of the bound S1 ubiquitin is predicted to be better conserved (Figure 5A) and was found to be highly predictive of the experimentally determined cleavage mode (Figures 5B and 5K). Interestingly, the M1-specific PcJOS and CsJOS demonstrate the existence of linkage specificity in Josephin-family clippases despite the spatial separation of cleavage and linkage. The direct comparison of PcJOS and BpJOS structures in complex with linear diubiquitin reveals the basis for the observed differences in linkage specificity. In PcJOS, the proximal M1-bound ubiquitin is recognized by an extensive S1′ interaction network. By contrast, the proximal ubiquitin of the BpJOS structure is completely disordered, probably due to the absence of an S1′-recognition interface, which is in line with the observed linkage promiscuity of BpJOS.

Besides their insights into DUB evolution and bacterial defense mechanisms, the Josephin-type clippases also offer possibilities for experimentally studying the ubiquitin system in general. Engineered multi-UBL clippase Lb^{pro*} has already been successfully applied to study branched ubiquitin chains.[20] After treatment with clippases, each ubiquitination site leaves a diGly remnant on a lysine residue, which can be identified using MS. In the case of ubiquitin, the detection of multiple remnants on a single ubiquitin unit proves the presence of branches and allows quantifying them.[20] However, Lb^{pro*} does not discriminate between ubiquitination, NEDDylation, and ISGylation, as all of these modifications are cleaved equally well. Moreover, being derived from a physiological deISGylase, Lb^{pro*} has no specificity for ubiquitin linkage types and thus does not yield information on the nature of the chain branches. Bacterial UCCs may be key to addressing these limitations. BpJOS is a highly active pan-linkage UCC that completely spares ISGylation sites (Figure S2C), allowing discrimination between ubiquitin- and ISG15-derived diGly remnants, which co-occur under stimulation of immunity. Since BpJOS also cleaves NEDD8-modifications in clippase mode, it cannot be used in its present form to discriminate between ubiquitination and NEDDylation sites. However, the structural data provided here should allow for the engineering of modifier-specific clippases. Another unique advantage of the bacterial Josephin-type clippases is the availability of linkage-specific enzymes. Among the eleven UCCs characterized in this study, five are highly active linkage-promiscuous enzymes, two are strictly M1-specific, and the rest exhibit modest linkage preferences without real specificity (Figures 1 and 5 and Boll et al.[18]). Current protein databases contain several dozen additional UCC candidates, and more bacterial sequences are being added continuously. The available sequence and structural diversity will be instrumental in the identification and engineering of additional clippases with new specificities.

Limitations of the study

The physiological targets of the enzymes described and their relevance to pathogenesis remain unknown. We can only speculate why UCCs are found in a small number of host-associated bacteria and are absent from major bacterial pathogens of medical importance. Although further enzymes with UCC activity may exist, UCC activity is probably detrimental to some aspects of bacterial fitness. These questions require further investigation. Our structural data and mutagenesis experiments suggest that the shift in UCC cleavage position relative to conventional Josephin-type DUBs is caused by different recognition of the distal (S1) ubiquitin. This preference is encoded within a short variable region of the catalytic domain, and structural prediction programs like AlphaFold can accurately predict UCC/DUB activity. Our failure to re-engineer the cleavage position by swapping variable regions was likely caused by insufficient structural stabilization to correctly position altered recognition loops. However, other factors may influence the cleavage position that are not fully understood.

RESOURCE AVAILABILITY

Lead contact

Further information and requests for resources and reagents should be directed to and will be fulfilled by the lead contact, Kay Hofmann (kay.hofmann@uni-koeln.de).

Materials availability

All reagents generated in this study will be made available on request, but we may require a payment and/or a completed materials transfer agreement if there is potential for commercial application.

Data and code availability

- All X-ray structures were deposited in the PDB database under accession numbers PDB: 9F5T (BpJOS), 9FN4 (PcJOS), 9FPA (PcJOS, orthorhombic), and 9G7G (PaJOS). The previously published structures 6PGV and 3O65 are also available from PDB. Raw data of mass spectroscopy were deposited with the ProteomeXchange database under the accession number PXD058333. Source data underlying the findings of this study have been deposited at Mendeley Data and are available from https://doi.org/10.17632/ggcmfjns65.1. All deposited data will be publicly available as of the date of publication.
- This paper does not report original code.
- Any additional information required to reanalyze the data reported in this paper is available from the lead contact upon request.

ACKNOWLEDGMENTS

We thank Christiane Horst for technical assistance. This work was supported by the DFG (grant HO 3783/3-2 to K.H.) and NWO (VIDI Grant VI. 213.110 to M.P.C.M). Crystals were grown using equipment of the Cologne Crystallization facility (C2f), supported by DFG Grant Inst 216/949-1 FUGG. Synchrotron data were collected at the Swiss Light Source, Paul Scherrer Institute, Switzerland, at beamline X06SA; the European Synchrotron Radiation Facility (ESRF), France, at beamline ID23_2; and PETRAIII, EMBL outstation, Hamburg, Germany, at beamline P13. We thank the staff for their support. We thank the CECAD Proteomics Facility (supported by DFG Grant Inst 216/1163-1 FUGG) for proteome data analysis.

AUTHOR CONTRIBUTIONS

T.H. and S.K. performed all biochemical and crystallization experiments. M.U. collected the X-ray data and solved the structure. U.B. supervised the

crystallography. R.A.d.H. and M.P.C.M. designed and synthesized activity-based probes. K.H. conceived and supervised the project and contributed bioinformatical analyses. All authors contributed to the manuscript.

DECLARATION OF INTERESTS

The authors declare no competing interests.

STAR★METHODS

Detailed methods are provided in the online version of this paper and include the following:

- KEY RESOURCES TABLE
- EXPERIMENTAL MODEL AND STUDY PARTICIPANT DETAILS
- METHOD DETAILS
  - Sequence Analysis
  - Cloning & Mutagenesis
  - Protein expression & purification
  - Enzymatic generation of activity-based probes
  - Chemical synthesis of activity-based probes
  - Chain generation
  - Intact mass analysis
  - Crystallization
  - Data collection, phasing, model building, and refinement
  - Activity-based probe assays
  - Ubiquitin chain cleavage
  - Cell culture and western blotting
  - Bottom-up proteomics for cleavage site determination
- QUANTIFICATION AND STATISTICAL ANALYSIS

SUPPLEMENTAL INFORMATION

Supplemental information can be found online at https://doi.org/10.1016/j.molcel.2025.02.002.

Received: July 24, 2024
Revised: December 5, 2024
Accepted: February 4, 2025
Published: March 3, 2025

REFERENCES

1. Squair, D.R., and Virdee, S. (2022). A new dawn beyond lysine ubiquitination. Nat. Chem. Biol. *18*, 802–811. https://doi.org/10.1038/s41589-022-01088-2.
2. Clague, M.J., Urbé, S., and Komander, D. (2019). Breaking the chains: deubiquitylating enzyme specificity begets function. Nat. Rev. Mol. Cell Biol. *20*, 338–352. https://doi.org/10.1038/s41580-019-0099-1.
3. Franklin, T.G., and Pruneda, J.N. (2021). Bacteria make surgical strikes on host ubiquitin signaling. PLOS Pathog. *17*, e1009341.
4. Zhou, Y., and Zhu, Y. (2015). Diversity of bacterial manipulation of the host ubiquitin pathways. Cell. Microbiol. *17*, 26–34. https://doi.org/10.1111/cmi.12384.
5. Roberts, C.G., Franklin, T.G., and Pruneda, J.N. (2023). Ubiquitin-targeted bacterial effectors: rule breakers of the ubiquitin system. EMBO J. *42*, e114318. https://doi.org/10.15252/embj.2023114318.
6. Pisano, A., Albano, F., Vecchio, E., Renna, M., Scala, G., Quinto, I., and Fiume, G. (2018). Revisiting bacterial ubiquitin ligase effectors: weapons for host exploitation. Int. J. Mol. Sci. *19*, 3576. https://doi.org/10.3390/ijms19113576.
7. Tripathi-Giesgen, I., Behrends, C., and Alpi, A.F. (2021). The ubiquitin ligation machinery in the defense against bacterial pathogens. EMBO Rep. *22*, e52864. https://doi.org/10.15252/embr.202152864.
8. Huang, J., and Brumell, J.H. (2014). Bacteria-autophagy interplay: a battle for survival. Nat. Rev. Microbiol. *12*, 101–114. https://doi.org/10.1038/nrmicro3160.
9. Walsh, S.C., Reitano, J.R., Dickinson, M.S., Kutsch, M., Hernandez, D., Barnes, A.B., Schott, B.H., Wang, L., Ko, D.C., Kim, S.Y., et al. (2022). The bacterial effector GarD shields Chlamydia trachomatis inclusions from RNF213-mediated ubiquitylation and destruction. Cell Host Microbe *30*, 1671–1684.e9. https://doi.org/10.1016/j.chom.2022.08.008.
10. Cui, J., Yao, Q., Li, S., Ding, X., Lu, Q., Mao, H., Liu, L., Zheng, N., Chen, S., and Shao, F. (2010). Glutamine deamidation and dysfunction of ubiquitin/NEDD8 induced by a bacterial effector family. Science *329*, 1215–1218. https://doi.org/10.1126/science.1193844.
11. Hermanns, T., and Hofmann, K. (2019). Bacterial DUBs: deubiquitination beyond the seven classes. Biochem. Soc. Trans. *47*, 1857–1866. https://doi.org/10.1042/BST20190526.
12. Kubori, T., Kitao, T., and Nagai, H. (2019). Emerging insights into bacterial deubiquitinases. Curr. Opin. Microbiol. *47*, 14–19. https://doi.org/10.1016/j.mib.2018.10.001.
13. Erven, I., Abraham, E., Hermanns, T., Baumann, U., and Hofmann, K. (2022). A widely distributed family of eukaryotic and bacterial deubiquitinases related to herpesviral large tegument proteins. Nat. Commun. *13*, 7643. https://doi.org/10.1038/s41467-022-35244-y.
14. Schubert, A.F., Nguyen, J.V., Franklin, T.G., Geurink, P.P., Roberts, C.G., Sanderson, D.J., Miller, L.N., Ovaa, H., Hofmann, K., Pruneda, J.N., et al. (2020). Identification and characterization of diverse OTU deubiquitinases in bacteria. EMBO J. *39*, e105127. https://doi.org/10.15252/embj.2020105127.
15. Pruneda, J.N., Durkin, C.H., Geurink, P.P., Ovaa, H., Santhanam, B., Holden, D.W., and Komander, D. (2016). The Molecular Basis for Ubiquitin and Ubiquitin-like Specificities in Bacterial Effector Proteases. Mol. Cell *63*, 261–276. https://doi.org/10.1016/j.molcel.2016.06.015.
16. Shin, D., Bhattacharya, A., Cheng, Y.L., Alonso, M.C., Mehdipour, A.R., van der Heden van Noort, G.J., Ovaa, H., Hummer, G., and Dikic, I. (2020). Bacterial OTU deubiquitinases regulate substrate ubiquitination upon Legionella infection. eLife *9*, e58277. https://doi.org/10.7554/eLife.58277.
17. Hermanns, T., Woiwode, I., Guerreiro, R.F., Vogt, R., Lammers, M., and Hofmann, K. (2020). An evolutionary approach to systematic discovery of novel deubiquitinases, applied to Legionella. Life Sci. Alliance *3*, e202000838. https://doi.org/10.26508/lsa.202000838.
18. Boll, V., Hermanns, T., Uthoff, M., Erven, I., Hörner, E.M., Kozjak-Pavlovic, V., Baumann, U., and Hofmann, K. (2023). Functional and structural diversity in deubiquitinases of the Chlamydia-like bacterium Simkania negevensis. Nat. Commun. *14*, 7335. https://doi.org/10.1038/s41467-023-43144-y.
19. Swatek, K.N., Aumayr, M., Pruneda, J.N., Visser, L.J., Berryman, S., Kueck, A.F., Geurink, P.P., Ovaa, H., van Kuppeveld, F.J.M., Tuthill, T.J., et al. (2018). Irreversible inactivation of ISG15 by a viral leader protease enables alternative infection detection strategies. Proc. Natl. Acad. Sci. USA *115*, 2371–2376. https://doi.org/10.1073/pnas.1710617115.
20. Swatek, K.N., Usher, J.L., Kueck, A.F., Gladkova, C., Mevissen, T.E.T., Pruneda, J.N., Skern, T., and Komander, D. (2019). Insights into ubiquitin chain architecture using Ub-clipping. Nature *572*, 533–537. https://doi.org/10.1038/s41586-019-1482-y.
21. Ekkebus, R., van Kasteren, S.I., Kulathu, Y., Scholten, A., Berlin, I., Geurink, P.P., de Jong, A., Goerdayal, S., Neefjes, J., Heck, A.J.R., et al. (2013). On terminal alkynes that can react with active-site cysteine nucleophiles in proteases. J. Am. Chem. Soc. *135*, 2867–2870. https://doi.org/10.1021/ja309802n.
22. Weeks, S.D., Grasty, K.C., Hernandez-Cuebas, L., and Loll, P.J. (2011). Crystal structure of a Josephin-ubiquitin complex: evolutionary restraints on ataxin-3 deubiquitinating activity. J. Biol. Chem. *286*, 4555–4565. https://doi.org/10.1074/jbc.M110.177360.

23. Seki, T., Gong, L., Williams, A.J., Sakai, N., Todi, S.V., and Paulson, H.L. (2013). JosD1, a membrane-targeted deubiquitinating enzyme, is activated by ubiquitination and regulates membrane dynamics, cell motility, and endocytosis. J. Biol. Chem. *288*, 17145–17155. https://doi.org/10.1074/jbc.M113.463406.

24. Grasty, K.C., Weeks, S.D., and Loll, P.J. (2019). Structural insights into the activity and regulation of human Josephin-2. J. Struct. Biol. X *3*, 100011. https://doi.org/10.1016/j.yjsbx.2019.100011.

25. De Cesare, V., Carbajo Lopez, D., Mabbitt, P.D., Fletcher, A.J., Soetens, M., Antico, O., Wood, N.T., and Virdee, S. (2021). Deubiquitinating enzyme amino acid profiling reveals a class of ubiquitin esterases. Proc. Natl. Acad. Sci. USA *118*, e2006947118. https://doi.org/10.1073/pnas.2006947118.

26. Hermanns, T., and Hofmann, K. (2023). Bioinformatical Approaches to the Discovery and Classification of Novel Deubiquitinases. Methods Mol. Biol. *2591*, 135–149. https://doi.org/10.1007/978-1-0716-2803-4_9.

27. Bucher, P., Karplus, K., Moeri, N., and Hofmann, K. (1996). A flexible motif search technique based on generalized profiles. Comput. Chem. *20*, 3–23.

28. Holm, L. (2020). Using Dali for Protein Structure Comparison. Methods Mol. Biol. *2112*, 29–42. https://doi.org/10.1007/978-1-0716-0270-6_3.

29. Engström, P., Burke, T.P., Tran, C.J., Iavarone, A.T., and Welch, M.D. (2021). Lysine methylation shields an intracellular pathogen from ubiquitylation and autophagy. Sci. Adv. *7*, eabg2517. https://doi.org/10.1126/sciadv.abg2517.

30. Puvar, K., Iyer, S., Fu, J., Kenny, S., Negrón Terón, K.I., Luo, Z.Q., Brzovic, P.S., Klevit, R.E., and Das, C. (2020). Legionella effector MavC targets the Ube2N∼Ub conjugate for noncanonical ubiquitination. Nat. Commun. *11*, 2365. https://doi.org/10.1038/s41467-020-16211-x.

31. Kozjak-Pavlovic, V., Herweg, J.A., and Rudel, T. (2018). The role of host cell organelles in the development of Simkania negevensis. Int. J. Med. Microbiol. *308*, 155–160. https://doi.org/10.1016/j.ijmm.2017.10.008.

32. Vandamme, P., Henry, D., Coenye, T., Nzula, S., Vancanneyt, M., LiPuma, J.J., Speert, D.P., Govan, J.R.W., and Mahenthiralingam, E. (2002). Burkholderia anthina sp. nov. and Burkholderia pyrrocinia, two additional Burkholderia cepacia complex bacteria, may confound results of new molecular diagnostic tools. FEMS Immunol. Med. Microbiol. *33*, 143–149. https://doi.org/10.1111/j.1574-695X.2002.tb00584.x.

33. Katoh, K., and Standley, D.M. (2013). MAFFT multiple sequence alignment software version 7: improvements in performance and usability. Mol. Biol. Evol. *30*, 772–780. https://doi.org/10.1093/molbev/mst010.

34. Schuepbach, T., Pagni, M., Bridge, A., Bougueleret, L., Xenarios, I., and Cerutti, L. (2013). pfsearchV3: a code acceleration and heuristic to search PROSITE profiles. Bioinformatics *29*, 1215–1217. https://doi.org/10.1093/bioinformatics/btt129.

35. Jumper, J., Evans, R., Pritzel, A., Green, T., Figurnov, M., Ronneberger, O., Tunyasuvunakool, K., Bates, R., Žídek, A., Potapenko, A., et al. (2021). Highly accurate protein structure prediction with AlphaFold. Nature *596*, 583–589. https://doi.org/10.1038/s41586-021-03819-2.

36. Niedermeyer, T.H.J., and Strohalm, M. (2012). mMass as a software tool for the annotation of cyclic peptide tandem mass spectra. PLOS One *7*, e44913. https://doi.org/10.1371/journal.pone.0044913.

37. Kabsch, W. (2010). Xds. Acta Crystallogr. D Biol. Crystallogr. *66*, 125–132. https://doi.org/10.1107/S0907444909047337.

38. McCoy, A.J., Grosse-Kunstleve, R.W., Adams, P.D., Winn, M.D., Storoni, L.C., and Read, R.J. (2007). Phaser crystallographic software. J. Appl. Crystallogr. *40*, 658–674. https://doi.org/10.1107/S0021889807021206.

39. Adams, P.D., Afonine, P.V., Bunkóczi, G., Chen, V.B., Davis, I.W., Echols, N., Headd, J.J., Hung, L.W., Kapral, G.J., Grosse-Kunstleve, R.W., et al. (2010). Phenix: a comprehensive Python-based system for macromolecular structure solution. Acta Crystallogr. D Biol. Crystallogr. *66*, 213–221. https://doi.org/10.1107/S0907444909052925.

40. Murshudov, G.N., Vagin, A.A., and Dodson, E.J. (1997). Refinement of macromolecular structures by the maximum-likelihood method. Acta Crystallogr. D Biol. Crystallogr. *53*, 240–255. https://doi.org/10.1107/S0907444996012255.

41. Emsley, P., Lohkamp, B., Scott, W.G., and Cowtan, K. (2010). Features and development of coot. Acta Crystallogr. D Biol. Crystallogr. *66*, 486–501. https://doi.org/10.1107/S0907444910007493.

42. Pape, T., and Schneider, T.R. (2004). HKL2MAP: a graphical user interface for macromolecular phasing with SHELX programs. J. Appl. Crystallogr. *37*, 843–844. https://doi.org/10.1107/S0021889804018047.

43. Langer, G., Cohen, S.X., Lamzin, V.S., and Perrakis, A. (2008). Automated macromolecular model building for X-ray crystallography using ARP/wARP version 7. Nat. Protoc. *3*, 1171–1179. https://doi.org/10.1038/nprot.2008.91.

44. Tyanova, S., Temu, T., and Cox, J. (2016). The MaxQuant computational platform for mass spectrometry-based shotgun proteomics. Nat. Protoc. *11*, 2301–2319. https://doi.org/10.1038/nprot.2016.136.

45. MacLean, B., Tomazela, D.M., Shulman, N., Chambers, M., Finney, G.L., Frewen, B., Kern, R., Tabb, D.L., Liebler, D.C., and MacCoss, M.J. (2010). Skyline: an open source document editor for creating and analyzing targeted proteomics experiments. Bioinformatics *26*, 966–968. https://doi.org/10.1093/bioinformatics/btq054.

46. Söding, J. (2005). Protein homology detection by HMM-HMM comparison. Bioinformatics *21*, 951–960. https://doi.org/10.1093/bioinformatics/bti125.

47. Berrow, N.S., Alderton, D., Sainsbury, S., Nettleship, J., Assenberg, R., Rahman, N., Stuart, D.I., and Owens, R.J. (2007). A versatile ligation-independent cloning method suitable for high-throughput expression screening applications. Nucleic Acids Res. *35*, e45. https://doi.org/10.1093/nar/gkm047.

48. Van Duyne, G.D., Standaert, R.F., Karplus, P.A., Schreiber, S.L., and Clardy, J. (1993). Atomic structures of the human immunophilin FKBP-12 complexes with FK506 and rapamycin. J. Mol. Biol. *229*, 105–124. https://doi.org/10.1006/jmbi.1993.1012.

49. El Oualid, F., Merkx, R., Ekkebus, R., Hameed, D.S., Smit, J.J., de Jong, A., Hilkmann, H., Sixma, T.K., and Ovaa, H. (2010). Chemical synthesis of ubiquitin, ubiquitin-based probes, and diubiquitin. Angew. Chem. Int. Ed. Engl. *49*, 10149–10153. https://doi.org/10.1002/anie.201005995.

50. Sakakibara, S. (1995). Synthesis of large peptides in solution. Biopolymers *37*, 17–28. https://doi.org/10.1002/bip.360370105.

51. Bremm, A., Freund, S.M.V., and Komander, D. (2010). Lys11-linked ubiquitin chains adopt compact conformations and are preferentially hydrolyzed by the deubiquitinase Cezanne. Nat. Struct. Mol. Biol. *17*, 939–947. https://doi.org/10.1038/nsmb.1873.

52. Komander, D., and Barford, D. (2008). Structure of the A20 OTU domain and mechanistic insights into deubiquitination. Biochem. J. *409*, 77–85. https://doi.org/10.1042/BJ20071399.

53. Vijay-Kumar, S., Bugg, C.E., and Cook, W.J. (1987). Structure of ubiquitin refined at 1.8 A resolution. J. Mol. Biol. *194*, 531–544. https://doi.org/10.1016/0022-2836(87)90679-6.

STAR★METHODS

KEY RESOURCES TABLE

REAGENT or RESOURCE	SOURCE	IDENTIFIER
Antibodies		
anti-Ubiquitin	Millipore	Cat#05-944; RRID:AB_441944
anti-Diglycyl-Lysine	Lucerna	Cat#30-0100
anti-β-Actin	Santa Cruz	Cat#sc-81178; RRID:AB_2223230
anti-Tubulin	Sigma-Aldrich	Cat#T6074; RRID:AB_477582
anti-DYKDDDDK HRP	Miltenyi Biotech	Cat#130-101-572; RRID:AB_2687602
anti-mouse HRP	Cell Signalling Technology	Cat#7076; RRID:AB_330924
Bacterial and virus strains		
E. coli DH5α	ThermoFisher	Cat#EC0112
E. coli Rosetta™(DE3)pLysS	Novagen	Cat#70956
Chemicals, peptides, and recombinant proteins		
K6-linked di-ubiquitin	Biomol GmbH	Cat#SBB-UP0060-C025
K29-linked di-ubiquitin	Biomol GmbH	Cat#SBB-UP0077-C025
K33-linked di-ubiquitin	Biomol GmbH	Cat#SBB-UP0066-C025
K27-linked di-ubiquitin	UbiQ	Cat#UbiQ-015
2Ub-K63-VME	UbiQ	Cat#UbiQ-087
Endoproteinase AspN	Promega	Cat#V1621
Deposited data		
Crystal structure of BpJOS	This study	PDB: 9F5T
Crystal structure of PcJOS	This study	PDB: 9FN4
Crystal structure of PcJOS (orthorhombic)	This study	PDB: 9FPA
Crystal structure of PaJOS	This study	PDB: 9G7G
Crystal structure of JOSD2	Grasty et al.[24]	PDB: 6PGV
Crystal structure of ATXN3L	Weeks et al[22]	PDB: 3O65
Bottom-up proteomics	This study	PRIDE: PpPXD058333
Source data	This study	https://doi.org/10.17632/ggcmfjns65.1
Experimental models: Cell lines		
HEK293T	ATCC	ATCC: CRL-3216
Oligonucleotides		
See Table S5 for a full list of oligonucleotides	This study	Table S5
Recombinant DNA		
See Table S5 for a full list of recombinant DNA	This study	Table S5
Software and algorithms		
MAFFT	Kathoh and Standley[33]	v7.505
Pftools	Bucher et al.[27]	v3
pfsearchV3	Schuepbach et al.[34]	v3
Alphafold	Jumper et al.[35]	v2.3
DALI	Holm[28]	online
mMass	Niedermeyer and Strohalm[36]	Version: 5.5
XDS	Kabsch[37]	Version: 20210323
PHASER	McCoy et al.[38]	Version: 2.8.3
phenix.refine	Adams et al.[39]	Version: 1.20_4478

(*Continued on next page*)

Continued

REAGENT or RESOURCE	SOURCE	IDENTIFIER
REFMAC	Murshudov et al.[40]	Version: 5.8.0425
COOT	Emsley et al.[41]	Version: 0.9.8.93
SHELX	Pape and Schneider[42]	ShelxC Version 2016/1 ShelxD Version 2013/2 ShelxE Version 2019/1
ArpWarp	Langer et al.[43]	Version: 8.0 patch 1
Pymol	DeLano Scientific LLC, Schrödinger Inc	Version: 1.8.6.2
ImageLab	Bio-Rad	Version: 5.2.1
MaxQuant	Tyanova et al.[44]	Version: 1.6.12.0
Skyline	Maclean et al.[45]	Version: 24.1

EXPERIMENTAL MODEL AND STUDY PARTICIPANT DETAILS

DH5α Escherichia coli (ThermoFisher) were used for all cloning and plasmid propagation. Rosetta™(DE3)pLysS E. coli (Novagen) were used for all recombinant protein expression. All E. coli strains were grown at 37°C in Luria-Bertani (LB) media containing appropriate antibiotics.

METHOD DETAILS

Sequence Analysis

Sequence alignments were generated using the MAFFT package.[33] Generalized profiles were derived from multiple alignments using pftools3[27] and searched against the UniProt database (https://www.uniprot.org) and NCBI microbial genome reference sequence database (https://www.ncbi.nlm.nih.gov/genome/microbes) using pfsearchV3.[34] HMM-to-HMM searches were performed using the HHSEARCH method.[46] All structural predictions were performed using the local installation of Alphafold 2.3.[35] For structural comparisons, the DALI software was used.[28]

Cloning & Mutagenesis

All coding regions of bacterial Josephin DUBs, except SnJOS2, were obtained by gene synthesis (IDT) and cloned into the pOPIN-S vector[47] using the In-Fusion HD Cloning Kit (Takara Clontech). SnJOS2 was amplified from *S. negevensis* genomic DNA (kind gift of Vera Kozjak-Pavlovic, Julius Maximilian University, Würzburg) and cloned accordingly. Codon-optimized diubiquitin was obtained by gene synthesis and cloned into the pOPIN-B vector.[47] Lbpro* was obtained via gene synthesis and cloned into the pOPIN-K vector.[47] DUB/UCC chimeras were designed in silico, obtained by gene synthesis, and cloned into the pOPIN-S vector[47] (Table S4). Point mutations were introduced using a QuikChange Lightning Kit (Agilent Technologies). Constructs for ubiquitin-PA purification (pTXB1-ubiquitin$^{1-75}$) and USP21 were kind gifts from David Komander (WEHI, Melbourne).

Protein expression & purification

Bacterial and human Josephins were expressed from the pOPIN-S vector with an N-terminal 6His-SMT3-tag. ISG15$^{79-165}$ and ubiquitin were expressed from the pOPIN-B vector and Lb^{pro*} was expressed from the pOPIN-K vector with an N-terminal 6His-tag or 6His-GST-tag, respectively. *Escherichia coli* (Strain: Rosetta (DE3) pLysS) were transformed with the respective constructs and 2-6 l cultures were grown in LB medium at 37 °C until an OD_{600} of 0.8 was reached. The cultures were cooled to 18 °C and protein expression was induced by addition of 0.1 mM isopropyl β-d-1-thiogalactopyranoside (IPTG).

The expression of selenomethionine-substituted PcJOS was carried out as described previously[48]: In brief, expression cultures were grown in M9 minimal medium supplemented with thiamine vitamin (0.0001% w/v final concentration) until an OD600 of 0.8 was reached. The cultures were mixed with feedback inhibition amino acid mix (0.5 g/l leucine, isoleucine, valine, selenomethionine, and 1 g/l lysine, threonine, and phenylalanine), induced with 0.2 mM IPTG, and cooled down to 18 °C. After 16 h, the cultures were harvested by centrifugation at 5000 × *g* for 15 min.

After 16 h, the cultures were harvested by centrifugation at 5000 × *g* for 15 min. After freeze-thawing, the pellets were resuspended in binding buffer (300 mM NaCl, 20 mM TRIS pH 7.5, 20 mM imidazole, 2 mM β-mercaptoethanol) containing DNase and lysozyme, and lysed by sonication using 10 s pulses at 50 W for a total time of 10 min. Lysates were clarified by centrifugation at 50,000 × *g* for 1 h at 4 °C, and the supernatant was used for affinity purification on HisTrap FF columns (GE Healthcare), according to the manufacturer's instructions. Except for ubiquitin and MxJOS, all 6His-Smt3, 6His-GSTand 6His-tags were removed by incubation with SENP1$^{415-644}$ or 3C protease, respectively. The proteins were dialyzed simultaneously in binding buffer. The liberated affinity tag and His-tagged SENP1 were removed by a second round of affinity purification using HisTrap FF columns (GE Healthcare). All proteins were purified by final size exclusion chromatography (HiLoad 16/600 Superdex 75pg) in 20 mM TRIS pH 7.5, 150 mM NaCl, and

2 mM dithiothreitol (DTT), concentrated using VIVASPIN 20 columns (Sartorius), flash frozen in liquid nitrogen, and stored at −80 °C. Protein concentrations were determined by measuring the absorption at 280 nm (A_{280}), using the extinction coefficients of the proteins derived from their sequences.

Enzymatic generation of activity-based probes

Wildtype Ub^{1-75}-PA, the R72A / R74A mutants and $ISG15^{79-154}$-PA were expressed as C-terminal intein fusion proteins. The intein fusion proteins were affinity-purified in buffer A (20 mM HEPES, 50 mM sodium acetate pH 6.5, 75 mM NaCl) from clarified lysates using Chitin Resin (New England Biolabs) following the manufacturer's protocol. On-bead cleavage was performed by incubation with cleavage buffer (buffer A containing 100 mM MesNa (sodium 2-mercaptoethanesulfonate)) for 24 h at room temperature (RT). The resin was washed extensively with buffer A, and the pooled fractions were concentrated and subjected to size exclusion chromatography (HiLoad 16/600 Superdex 75pg) with buffer A. Propargylated probes were synthesized by reacting 300 μM Ub/Ubl-MesNa with 600 mM propargylamine hydrochloride (Sigma Aldrich) in buffer A containing 150 mM NaOH for 3 h at RT. Unreacted propargylamine was removed by size exclusion chromatography, and the probes were concentrated using VIVASPIN 20 columns (3 kDa cutoff, Sartorius), flash frozen, and stored at −80 °C.

Chemical synthesis of activity-based probes

Ub^{1-73} and $Nedd8^{1-73}$ were synthesized on a Syro II MultiSyntech Automated Peptide synthesizer using standard 9-fluorenylmethoxycarbonyl (Fmoc)-based solid-phase peptide chemistry on a 20 μmol scale as described previously.[49] Here, the N-terminal methionine (and position 50 methionine in Nedd8) was replaced with the known isostere norleucine. After N-terminal Boc protection, sidechain-protected Ub or Nedd8 was released from the resin using HFIP/DCM (2.5 ml, 1/4, v/v, 3x 20 min). The cleaved peptide (10 μmol) was dissolved in TFE/$CHCl_3$ (6 ml, 1/1, v/v) and cooled to -10°C to prevent racemization.[50] PA (6.40 μl, 100 μmol, 5 eq.), EDC.HCl (19.2 mg, 100 μmol, 5 eq.), and HOBt (15.3 mg, 100 μmol, 5 eq.) was added and stirred for 10 min at -10°C, then overnight at RT. After confirming full conversion, the excess solvent was evaporated, and global deprotection was performed with TFA/Tis/H_2O/Phenol (6 ml, 90/2.5/5/2.5, v/v) for 3 h. The mixture was added to cold ether/pentane (40 ml, 1/3, v/v) to precipitate the product, which was isolated by centrifugation (3500 rpm, 5 min, 4°C) and washed with cold diethyl ether (3x). The pellet was re-dissolved in DMSO (1.5 ml) and diluted in water (40 ml) for purification by RP-HPLC. The pure fractions were lyophilized to obtain the title compounds Ub^{1-73}-PA and $Nedd8^{1-73}$-PA as white powders. Ub^{1-73}-PA (7.15 mg, 0.86 μmol, 8.6%). MS ES+ (amu) calculated: M+H+ = 8314 Da, deconvoluted mass found: M+H+ = 8314 Da. $Nedd8^{1-73}$-PA. MS ES+ (amu) calculated: M+H+ = 8289 Da, deconvoluted mass found: M+H+ = 8289 Da.

Chain generation

Untagged Met1-linked diubiquitin was expressed as a linear fusion protein and purified using ion exchange chromatography and size-exclusion chromatography. Wild-type 6His-tagged Met1-linked diubiquitin and mutants were expressed as linear fusion proteins and purified using HisTrap affinity purification and size exclusion chromatography. K11-, K48-, and K63-linked ubiquitin chains were enzymatically assembled using UBE2SΔC (K11), CDC34 (K48), and Ubc13/UBE2V1 (K63) as previously described.[51,52] In brief, ubiquitin chains were generated by incubation of 1 μM E1, 25 μM of the respective E2, and 2 mM ubiquitin in reaction buffer (10 mM ATP, 40 mM TRIS (pH 7.5), 10 mM $MgCl_2$, and 1 mM DTT) for 18 h at RT. The respective reactions were stopped by a 20-fold dilution in 50 mM sodium acetate (pH 4.5), and chains of different lengths were separated by cation exchange using a Resource S column (GE Healthcare). The elution of different chain lengths was achieved with a gradient from 0 to 600 mM NaCl.

Intact mass analysis

Samples were analyzed at the Proteomics Facility (CECAD, Cologne) on a Shimadzu Nexera X2 coupled to a TripleTOF 6600 using a DuoSpray ion source heated to 150 °C (both Sciex). Samples were separated on a Jupiter C4 column (150 cm length, 1 mm inner diameter, Phenomenex) using a 5 min isocratic gradient of 20 % acetonitrile with 0.2 % formic acid. After 5 min, washing was performed by increasing the acetonitrile concentration to 85 % for 3 min, followed by re-equilibration to the initial conditions. Acquisition was performed in positive MS1 between 600 and 1600 m/z, with a de-clustering potential of 10. System control and data acquisition were performed using Analyst TF 1.8.1, which was also used to export the integrated spectra of the relevant peaks. Afterwards, annotation of monoisotopic masses and subsequent deconvolution of charge clusters were performed in mMass 5.5.[36]

Crystallization

Catalytically inactive PcJOS (± selenomethionine substitution) and linear-linked diubiquitin were mixed in a 1:1.1 ratio and crystallized using sitting drop vapor diffusion with commercially available sparse matrix screens. 96 well crystallization plates containing 30 μL of the respective screening conditions were mixed with 10 mg/ml protein in ratios of 1:2, 1:1, and 2:1 in 300 nl drops. Initial crystals of the native complex appeared in MIDAS G6 (35 % v/v glycerol ethoxylate, 0.2 M lithium citrate) at 20°C and were cryoprotected with perfluoropolyether. The best diffracting crystals of the selenomethionine-substituted complex were harvested from Morpheus B7.

PaJOS (100 μM) was incubated with 200 μM ubiquitin-PA for 18 hours at 4 °C. Unreacted PaJOS and Ub-PA were removed by size-exclusion chromatography. The covalent PaJOS/Ub-PA complex (10 mg/ml) was crystallized via vapor diffusion with commercially available sparse-matrix screens. Crystallization trials were set up with drop ratios of 1:2, 1:1, and 2:1 protein solution to precipitant

solution with a total volume of 300 nl. Initial crystals appeared in Crystal A6 (0.2 M magnesium chloride, 0.1 M TRIS pH 8.5, 30 % w/v PEG4000) at 20°C. These crystals were optimized by gradually changing the pH and PEG4000 concentration using 48-well MRC plates with 80 μl reservoir solutions and 3 μl drops (protein/precipitant ratios: 2:1, 1:1, and 1:2). The best diffracting crystals were harvested from a condition containing 0.2 M magnesium chloride, 0.1 M TRIS pH 9, and 30 % w/v PEG4000.

Catalytically inactive BpJOS and linear-linked diubiquitin were mixed in a 1:1.1 ratio and crystallized using sitting drop vapor diffusion with commercially available sparse matrix screens. 96 well crystallization plates containing 30 μL of the respective screening conditions were mixed with 10 mg/ml protein in ratios of 1:2, 1:1, and 2:1 in 300 nl drops. Initial crystals of the native complex appeared in Wizard A1 (20 % w/v PEG8000, 0.1 M CHES pH 9.5) at 20°C. These crystals were optimized by gradually changing the pH and PEG8000 concentration using 48-well MRC plates with 80 μl reservoir solutions and 3 μl drops (protein/precipitant ratios: 2:1, 1:1, and 1:2). Best diffracting crystals were harvested from a condition containing 0.1 M CHES pH 9.5; 22 % w/v PEG8000 and were cryoprotected with reservoir solution containing 20 % w/v glycerol.

Data collection, phasing, model building, and refinement

All diffraction data were processed using XDS.[37] Molecular replacement structure solution was performed using PHASER.[38] Refinement was achieved by phenix.refine and refmac and model building using the program COOT.[39–41] The tetragonal crystal form of PcJOS was used for selenomethionine phasing, with data collected at beamline X06SA, Swiss Light Source, Paul Scherrer Institute, Villigen, Switzerland. Phasing was achieved by SHELX, and initial automatic model building by ArpWarp.[42,43] The orthorhombic crystal form of PcJOS was solved by molecular replacement using PHASER[38] and the model from the tetragonal crystal form with data from beamline ID23_2 at ESRF, Grenoble, France. For PaJOS, data were also collected at beamline X06SA at the Swiss Light Source. The structure was solved by molecular replacement using a search model predicted by AlphaFold 2.3[35] and ubiquitin (entry 1UBQ).[53] The structure of BpJOS was likewise determined using AlphaFold and PHASER with data from beamline P13 at PETRAIII, EMBL outstation, in Hamburg, Germany. The data collection and refinement statistics are provided in Tables S2 and S3.

Activity-based probe assays

DUBs or UCCs were prediluted to a 2× concentration (10 μM) in reaction buffer (20 mM TRIS pH 7.5, 150 mM NaCl, and 10 mM DTT) and combined 1:1 with 100 μM activity-based probes for 18 h at 20°C. The deviating time points are indicated in the respective legends. The reaction was stopped by the addition of 2x Laemmli buffer and analyzed by SDS-PAGE using Coomassie staining.

Ubiquitin chain cleavage

DUBs were prediluted in 150 mM NaCl, 20 mM TRIS pH 7.5, and 10 mM DTT. The cleavage was performed at 20°C for the indicated time points with different DUB concentrations (PcJOS/BpJOS: 50 nM, PaJOS: 0.5 μM or as indicated in the respective figure legends) and 25 μM diubiquitin (M1, K11, K48, K63 synthesized as described above, K6, K29, K33 purchased from Biomol, K27 from UbiQ) or 20 μM Ub6+ chains (K63; synthesized as described above). The reactions were stopped with 2x Laemmli buffer, resolved by SDS-PAGE, and either Coomassie stained or transferred to PVDF membranes by western blotting.

Cell culture and western blotting

HEK293T cells obtained from ATCC were cultured at 37°C and 5 % CO2 in Dulbecco's modified Eagle's medium (DMEM; Gibco), supplemented with 10 % fetal calf serum (FCS) and 1 % penicillin-streptomycin. The cells were grown to 90 % confluence before harvesting. The collected cell pellets were resuspended in lysis buffer (20 mM Tris pH 7.5, 150 mM NaCl, 0.5 % NP-40, 2 mM EDTA, and 5 mM NEM) and sonicated with 3x 10s pulses. Cell debris were cleared by centrifugation at 16,000 × g for 15 min at 4°C. Protein concentration was quantified using a Bradford assay (Roti Quant; Roth) and adjusted to 5 μg/μl total protein content. Unreacted NEM was quenched with 10 mM DTT. Cell lysates were incubated with 10 μM of the corresponding enzymes (BpJOS, BcJOS, PcJOS$^{70\text{-}324}$, HeJOS, PaJOS, USP21$^{196\text{-}565}$, ATXN3L, and JOSD2) for the indicated times. The reaction was quenched by addition of 2x or 5x Laemmli buffer and boiling of the samples at 95°C for 5 min. Samples were resolved on a 12% Tris-glycine gel and transferred onto PVDF membranes by semi-dry western blotting. Membranes were decorated with primary antibodies overnight at 4°C: anti-Ubiquitin (Millipore, 05-944, 1:3000), anti-Diglycyl-Lysine (Lucerna, GX41, 1:500), anti-β-Actin (Santa Cruz, sc-81178, 1:500), anti-Tubulin (Sigma-Aldrich, T6074, 1:5000) or for 1h at RT (anti-DYKDDDDK HRP, Miltenyi Biotech, 130-101-572, 1:10000). Secondary HRP-linked antibody was incubated (anti-mouse, Cell Signaling Technology, Cat#7076, 1:3000 in 5% milk in PBS-T) for 1h at RT. HRP secondary antibodies were developed using the WesternBright chemiluminescent reagent (Advansta, K-12045). Gel images were acquired using ImageLab software 5.2.1.

Bottom-up proteomics for cleavage site determination

Lys63-linked diubiquitin chains (10 μg) were incubated with 5 μM SnJOS1 in 50 mM ABC buffer. The reaction was quenched after 16 h at RT by urea denaturation and supplemented with DTT (5 mM final concentration) and CAA (40 mM final concentration). The urea concentration was diluted to >0.8 M with 50 mM ABC buffer. Protein digestion with AspN (Promega, V1621) was performed at an 1:40 enzyme to substrate ratio for 16 h at 37 °C. The reaction was acidified with formic acid (1 % final concentration) and the peptides were purified on an SDB RP StageTip. Samples were analyzed at the CECAD Proteomics Facility on an Orbitrap Exploris 480 (Thermo Scientific) mass spectrometer that was coupled to an Vanquish neo in trap-and-elute setup (Thermo Scientific). Samples were loaded

onto a precolumn (Acclaim 5μm PepMap 300 μ Cartridge) with a flow of 60 μL/min before reverse-flushing onto an in-house packed analytical column (30 cm length, 75 μm inner diameter, filled with 2.7 μm Poroshell EC120 C18, Agilent). Peptides were chromatographically separated with an initial flow rate of 400 nL/min and the following gradient: initial 2% B (0.1% formic acid in 80 % acetonitrile) up to 6 % in 3 min. Then, the flow was reduced to 300 nl/min and B increased to 20% B in 26 min, up to 35% B within 15 min, and up to 98% solvent B within 1.0 min while again increasing the flow to 400 nl/min, followed by column washing with 95% solvent B and re-equilibration to the initial condition. The mass spectrometer was operated in data-dependent acquisition with a cycle time of 1 s, with MS1 scans acquired from 350 m/z to 1400 m/z at 60k resolution and an AGC target of 300%. MS2 scans were acquired at a resolution of 15 k with a maximum injection time of 118 ms, a normalized AGC target of 50% in a 2 Th window and a fixed first mass of 110 m/z. All MS1 scans were stored as profile, all MS2 scans as centroid. RAW data were analyzed using MaxQuant 1.6.12.0[44] and the spectra were visualized using Skyline.[45]

QUANTIFICATION AND STATISTICAL ANALYSIS

Intact mass spectrometry data were quantified using mMass software v5.5.[36] No statistical analyses are presented.